



University of Kerbala
College of Science
Department of Chemistry

Synthesis , Characterization of Silica-Metal Nanoparticles Via Sol–Gel Method and Studying Their Biological Activity

A Thesis

**Submitted to the College of Science /University of Kerbala in Partial
Fulfillment of the Requirement for the Degree of Master of Science in
Chemistry**

By

Khudair Rasheed Kitab

B.Sc. University of Kerbala (2007)

Supervised By

Prof. Dr. Hayder Hamied Mihsen

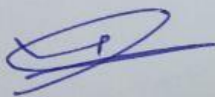
بِسْمِ اللَّهِ الرَّحْمَنِ الرَّحِيمِ

أَقْرَأْ بِاسْمِ رَبِّكَ الَّذِي خَلَقَ ١
خَلَقَ الْإِنْسَانَ مِنْ عَلَقٍ ٢ أَقْرَأْ وَرَبُّكَ
الْأَكْرَمُ ٣ الَّذِي عَلَّمَ بِالْقَلَمِ ٤
عَلَّمَ الْإِنْسَانَ مَا لَمْ يَعْلَمْ ٥

صدق الله العلي العظيم سورة العلق الآيات (1-5)

Supervisors Certification

I certify that this thesis " **Synthesis , Characterization of Silica-Metal Nanoparticles Via Sol–Gel Method and Studying Their Biological Activity** " was conducted under my supervision at the Department of Chemistry, College of Science, University of Kerbala, as a partial fulfillment of the requirements for the degree of Master of Science in Chemistry.



Signature:

Name: **Dr. Hayder Hamied Mihsen**

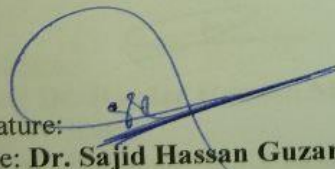
Title: Professor

Address: University of Kerbala,
College of Science, Department of
Chemistry

Date: / /2025

Report of the Head of the Chemistry Department

According to the recommendations presented by the Supervisors and the Postgraduate Studies Director, I forward this thesis " **Synthesis , Characterization of Silica-Metal Nanoparticles Via Sol-Gel Method and Studying Their Biological Activity**" for examination.

Signature: 

Name: **Dr. Sajid Hassan Guzar**

Title: Professor.

Head of Chemistry Department

Address: University of Kerbala, College of Science, Department of Chemistry.

Date: / /2025

Examination Committee Certification

We, the examining committee, certify that we have read this thesis and examined the student (**Khudair Rasheed Kitab**) in its contents and that in our opinion; it is adequate as a thesis for the degree of Master of Science in Chemistry.

S.T. Saad

Signature:

Name: **Dr. Suad Taha Saad**

Title: Assistance Professor

Address: University of Babylon, College of Science for Women , Department of Chemistry

Date: / / 2025

(Chairman)

Signature:

Name: **Dr. Jihan Hameed Abdulameer**

Title: Assistance Professor

Address: University of Karbala, College of Education for Pure Sciences, Department of Chemistry.

Date: 13 / 3 / 2025

(Member)

Signature:

Name: **Dr. Atheer Hasan Yas**

Title: Lecturer

Address: University of Kerbala, College of Science, Department of Chemistry.

Date: 13 / 3 / 2025

(Member)

Signature:

Name: **Dr. Hayder Hamied Mihsen**

Title: Professor

Address: University of Kerbala, College of Science, Department of Chemistry.

Date: / / 2025

(Member & Supervisor)

Approved by the council of the College of Science

Signature: Hassan Jameel Jawad ALfatlawy

Name: **Dr. Hassan Jameel Jawad ALfatlawy**

Title: Professor

Address: Dean of College of Science, University of Kerbala.

Date: / / 2025

Dedication

Loyalty requires that credit be given to those who deserve it, so I dedicate this work to the one who, after God, had the credit for producing this scientific research, Professor Dr. Hayder Hamied Mihsen, for his kindness in supervising this thesis, and in whom I found a virtuous and generous professor, who made an effort and provided sound guidance and sound opinion, which helped me overcome many difficulties. May God reward him with the best reward.

To the one whom God has crowned with awe and reverence and taught me to give without expectation and whose name I carry with all pride, my dear father, the dearest departed to my heart and the most present absent person in my memory.

May God have mercy on you, my dear father.

To the one who stays awake nights and days for me to my dear mother.

To my brother.... my support, my strength, and the one who shares my joys and sorrows.

To my wife.... the highest symbol of loyalty and faithfulness and my companion on the path.

To my children.... the apple of my eye.

To all my friends, I dedicate this scientific research .

Acknowledgement

Initially, I want to thank the almighty Allah for giving me the strength and guidance throughout my entire life and during this work in particular. I wish also to express my deepest gratitude to my supervisor **Prof. Dr. Hayder Hamied Al-Hmedawi** for his continuous support, invaluable suggestions and great contributions since the very beginning of this work.

Also, I want to thank all faculty members of Department of Chemistry in the College of Science at The University of Kerbala, for their precious support. Finally, I want to thank my family and friend for their continual support throughout this journey. They were my source of encouragement along the way.

KHUDIR

Abstract

This study involved the use of rice husks to produce four metal-silica nanoparticles compounds ($\text{SiO}_2\text{@Ni(II)}$, $\text{SiO}_2\text{@Ni(0)}$, $\text{SiO}_2\text{@Cu(II)}$, and $\text{SiO}_2\text{@Cu(0)}$) with high capacity to inhibit certain two types of bacteria *Escherichia coli* (*E.Coli*) and *Staphylococcus aureus* (*S.aureus*) that are harmful to human health.

In the first step, sodium silicate solution was prepared from rice husks, then silica was functionalized with nickel and copper ions by adding nickel nitrate hexahydrate to produce $\text{SiO}_2\text{@Ni(II)}$ and copper nitrate trihydrate to produce $\text{SiO}_2\text{@Cu(II)}$ via the sol-gel method. Then, the prepared compounds were reduced with a reducing agent, sodium borohydride, to prepare $\text{SiO}_2\text{@Ni(0)}$ and $\text{SiO}_2\text{@Cu(0)}$ nanoparticles. The prepared compounds were characterized using several techniques (FTIR, XRD, FESEM-EDX, XPS, AFM, TEM, and TGA/DTA). Samples of bacteria isolated using conventional methods were collected from Al-Husseini Teaching Hospital in Karbala and these strains were chemically characterized using the API staph system applied according to the manufacturer's instructions. The nanocomposites prepared from rice husks ($\text{SiO}_2\text{@Ni(II)}$, $\text{SiO}_2\text{@Ni(0)}$, $\text{SiO}_2\text{@Cu(II)}$, and $\text{SiO}_2\text{@Cu(0)}$) were tested against bacteria (*E.Coli* and *S.aureus*) at dilute concentrations (20, 40, 60, 80, 100) mg/mL and compared with DMSO as a negative control. It was found that the inhibitory effect of the studied compounds increases with increasing concentration. It was also found that bacterial growth occurs at low concentrations of nanoparticles compared to the studied compounds at High concentrations. From the diameters of inhibition, it appears that inhibition of *S. aureus* is somewhat higher than inhibition of *E. coli*.

Table of Contents		
Summary		I
Table of contents		II
List of Figures		III
List of Schemes		V
List of Tables		VI
List of Abbreviations and Symbols		VII
1. Introduction		
1.1 Rice husk		1
1.2 Extraction of silica from rice husk		3
1.3 silica		5
1.4 surface of silica		7
1.5 Polysiloxane		8
1.6 Sol–gel method		10
1.7 Modification of The Surface of Silica With Metal Ions		13
1.8 Nickel and copper		16
1.9 Biological activity of (metals-silica) materials		19
1.10 The Aims		23
2. Experimental Part		24
2.1 Instruments		24
2.2 Materials		25
2.3 The preparation methods		25
2.3.1 . Preparation of sodium silicate solution from rice husks		25
2.3.2 Preparation of nickel silica nanoparticles $\text{SiO}_2@\text{Ni(II)}$		26
2.3.3 Preparation of nickel silica nanoparticles $\text{SiO}_2@\text{Ni(0)}$		26
2.3.4 Preparation of copper silica nanoparticles $\text{SiO}_2@\text{Cu(II)}$		27
2.3.5. Preparation of copper silica nanoparticles $\text{SiO}_2@\text{Cu(0)}$		27
2.3.6 Antimicrobial Assay		28
2.3.6.1 Bacterial Isolate		28
2.3.6.2 Antibacterial activity of silica nanoparticles		29
3. Results and Discussion		
3.1. Synthesis and characterization of $\text{SiO}_2@\text{Ni(II)}$ and $\text{SiO}_2@\text{Ni(0)}$		30
3.1.1. Fourier transform infrared spectroscopy (FTIR)		31

3.1.2	X-ray diffraction Analysis (XRD)	32
3.1.3	N ₂ Adsorption–Desorption Analysis	32
3.1.4	Field emission scanning electron microscopy (FESEM) analysis	33
3.1.5	Transmission Electron Microscopy (TEM) analysis	34
3.1.6	Atomic Force Microscopy (AFM)	35
3.1.7	Thermogravimetric Analysis (TGA-DSC)	36
3.1.8	UV–Vis (DRUV–Vis) absorption spectra	37
3.1.9	X-ray photoelectron spectroscopy (XPS)	39
3.1.10	Evaluation of Antibacterial Activity	40
3.2	Synthesis and characterization of SiO ₂ @Cu(II) and SiO ₂ @Cu(0)	44
3.2.1	Fourier transform infrared spectroscopy (FTIR)	45
3.2.2	X-ray diffraction Analysis (XRD)	46
3.2.3	N ₂ Adsorption–Desorption Analysis	45
3.2.4	Field emission scanning electron microscopy (FESEM) analysis	48
3.2.5	Transmission Electron Microscopy (TEM) analysis	49
3.2.6	Atomic Force Microscopy (AFM)	49
3.2.7	Thermogravimetric Analysis (TGA-DSC)	50
3.2.8	UV–Vis (DRUV–Vis) absorption spectra	51
3.2.9	Evaluation of Antibacterial Activity	53
4.	Conclusion	57
5.	Future works	58
	References	59
List of Figures		
Figure 1. 1:	Rice grain and respective structures, and rice husk	1
Figure 1. 2:	(a) Rice Husk (b) Rice Husk Ash (c) Rice Husk Silica Powder.	4
Figure 1. 3:	Diagram of the procedure was used to extract silica powders from RHA.	4
Figure 1. 4:	The linear structure of silicon dioxide (SiO ₂).	5
Figure 1. 5 :	The crystal structure of Silicon Dioxide.	6
Figure 1. 6:	Different types of silanol group on the surface of silica.	7
Figure 1. 7 :	Q _n nomenclature used to define the environment of the silicon	8

atoms in silica.	
Figure 1. 8 : Structure of Polysiloxane.	10
Figure 1. 9 :The diagram of sol-gel method to yield a dry material (xerogel or aerogel).	12
Figure 1. 10 : The process of sol-gel	13
Figure 1. 11: show the Nickel as element with chemical in formation.	17
Figure 1. 12: illustration of the synthetic procedure for SiO ₂ @Ni and hollow Ni microspheres.	17
Figure 1. 13: show the Copper as element with chemical in formation.	18
Figure 1 .14: Mechanism for antibacterial activity of copper nanoparticles	19
Figure 1 .15: Mechanism for antibacterial activity of nickel nanoparticles	20
Figure 3. 1: FTIR spectra of SiO ₂ @Ni(II) and SiO ₂ @Ni(0)	31
Figure 3. 2: The XRD pattern of SiO ₂ @Ni(II) and SiO ₂ @Ni(0)	32
Figure 3. 3: The nitrogen adsorption–desorption isotherms of (A) SiO ₂ @Ni(II) and (B) SiO ₂ @Ni(0). The inset shows the corresponding pore size distribution	33
Figure 3. 4: A & B FESEM-EDX for SiO ₂ @Ni(II), C & D FESEM-EDX for SiO ₂ @Ni(0)	34
Figure 3. 5: A The TEM image of SiO ₂ @Ni(II) and B The TEM image of SiO ₂ @Ni(0)	35
Figure 3. 6: A & B Two-dimensional and three-dimensional images of SiO ₂ @Ni(II),C & D Two-dimensional and three-dimensional images of SiO ₂ @Ni(0).	36
Figure 3. 7: TGA/DSC analysis of (A) SiO ₂ @Ni(II) and (B) SiO ₂ @Ni(0)	37
Figure 3. 8 DRUV–vis spectra of SiO ₂ @Ni(II) and (B) SiO ₂ @Ni(0) composites	37
Figure 3. 9: The O 1s (A), Si 2p (B) and Ni 2p (C) X-ray photoelectron spectra of nickel-silica nanoparticles SiO ₂ @Ni(II) and (B) SiO ₂ @Ni(0)	40
Figure 3. 10: Antibacterial activity of nickel-silica nanoparticles SiO ₂ @Ni(II) and SiO ₂ @Ni(0) against <i>E.coli</i> and <i>S.aureus</i> in different concentrations 20, 40, 60, 80 and 100 mg/mL.	43
Figure 3. 11: FTIR spectra of SiO ₂ @Cu(II) and SiO ₂ @Cu(0)	45
Figure 3. 12: The XRD pattern of SiO ₂ @Cu(II) and SiO ₂ @Cu(0)	46

Figure 3.13: The N ₂ adsorption/desorption isotherms of (A) SiO ₂ @Cu(II) and (B) SiO ₂ @Cu(0). The inset shows the corresponding pore size distribution.	47
Figure 3.14: A & B FESEM-EDX for SiO ₂ @Cu(II), C & D FESEM-EDX for SiO ₂ @Cu(0)	48
Figure 3.15: A The TEM images of A- SiO ₂ @Cu(II) and B- SiO ₂ @Cu(0)	49
Figure 3.16: A & B Two-dimensional and three-dimensional images of SiO ₂ @Cu(II), C & D Two-dimensional and three-dimensional images of SiO ₂ @Cu(0).	50
Figure 3.17: TGA/DSC analysis of (A) SiO ₂ @Cu(II) and (B) SiO ₂ @Cu(0)	51
Figure 3.18: DRUV-vis spectra of SiO ₂ @Cu(II) and (B) SiO ₂ @Cu(0) composites	53
Figure 3-19: Antibacterial activity of nickel-silica nanoparticles SiO ₂ @Cu(II) and SiO ₂ @Cu(0) against <i>E.coli</i> and <i>S.aureus</i> in different concentrations 20, 40, 60, 80 and 100 mg/mL.	56

List of Schemes	
Scheme 1-1 : The suggested reactions of the hydrolysis and condensation processes that occur in the sol-gel method.	11
Scheme 1-2: Silica surface modification	15
Scheme 2-1: Preparation of nickel-silica nanoparticles SiO ₂ @Ni(II), SiO ₂ @Ni(0) and copper-silica nanoparticles SiO ₂ @Cu(II), SiO ₂ @Cu(0) from rice husk	28
Scheme 3-1: Preparation of SiO ₂ @Ni(II) and SiO ₂ @Ni(0) from rice husk	30
Scheme 3-2: Preparation of SiO ₂ @Cu(II) and SiO ₂ @Cu(0) from rice husk	44

List of Tables	
Table 1.1: Chemical analysis of the raw RH.	3
Table 2.1: List of instruments, supplier companies and place of measurement..	24
Table 2.2: Chemicals used in this work and their provider.	25
Table 3.1 The result of N ₂ - adsorption/desorption analysis of SiO ₂ @Ni(II) and SiO ₂ @Ni(0)	33
Table 3.2: Roughness parameters of SiO ₂ @Ni(II) and SiO ₂ @Ni(0)	36
Table 3.3: The antibacterial effect of SiO ₂ @Ni(II) and SiO ₂ @Ni(0) against <i>E. coli</i> and <i>S. aureus</i>	42
Table 3.4: Minimum inhibitory concentration (MIC) mg/mL for SiO ₂ @Ni(II) and SiO ₂ @Ni(0) against <i>E. coli</i> and <i>S. aureus</i> .	43
Table 3.5: The result of N ₂ - adsorption/desorption analysis of SiO ₂ @Cu(II) and SiO ₂ @Cu(0)	47
Table 3.6: Roughness parameters of SiO ₂ @Cu(II) and SiO ₂ @Cu(0)	50
Table 3.7: The antibacterial activity of SiO ₂ @Cu(II) and SiO ₂ @Cu(0) against <i>E. coli</i> and <i>S. aureus</i> .	55
Table 3.8: Minimum inhibitory concentration (MIC) mg/mL for SiO ₂ @Cu(II) and SiO ₂ @Cu(0) against <i>E. coli</i> and <i>S. aureus</i>	56

List of Abbreviations and Symbols

symbols	Name
%	Percentage
°C	Degree Celsius
AFM	Atomic Force Microscope
FTIR	Fourier-transform infrared spectroscopy
BET	Brunauer-Emmett-Teller
FESEM	Field Emission Scanning Electron Microscopy
DMSO	Di methyl sulfoxide
RH-SiO ₂ @Ni(II)	Rice Husk Silica – Di Nickel
RH-SiO ₂ @Cu(II)	Rice Husk Silica- Di copper
TEM	Transmission electron microscopy
h	Hour
IUPAC	International Union of Pure and Applied Chemistry
XPS	X-ray photoelectron spectroscopy
Me	Metal
M	Molar
mol	Mole
RH-SiO ₂ @Ni(0)	Rice Husk Silica –Nickel
RH-SiO ₂ @Cu(0)	Rice Husk Silica- copper
TGA	Thermo gravimetric Analysis
UV-Vis	UV–Vis (DRUV–Vis) absorption spectra
ICP-MS	inductively coupled plasma mass spectrometry
XRD	X-ray diffraction

CHAPTER ONE

INTRODUCTION

1 Introduction

1.1 Rice husk

Rice is a type of grass seed that comes from the *Oryza sativa* species, which is commonly referred to as Asian rice, or the *Oryza glaberrima* species, that is also called African rice [1]. Often a staple in many nations, rice is a food that is produced widely all over the world. Consequently, an extensive research program to boost rice output has started and considered is the second most consumed food in the world after wheat, with annual global supply of roughly 471 million tonnes and average per capita consumption of around 57 kg a year[2]. Rice husk (RH) is the most representative by-product of industrial rice production. Rice culture stands by the region of manufacturing and cultivation, playing a strategic role in the world economy. The outer layer of rice is referred to as the "rice husk." During the milling process, rice husk and grains are typically kept apart. Hull makes up 20% of the paddy's weight. There are four different types of rice husk layers: cellular, sponge-like, fibrous, and structural[3], as shown in Figure (1-1). Rice husks are generally considered to be a waste material that should be burned or disposed of in a landfill. But nowadays, rice husks are thought of as a product that can be sold.

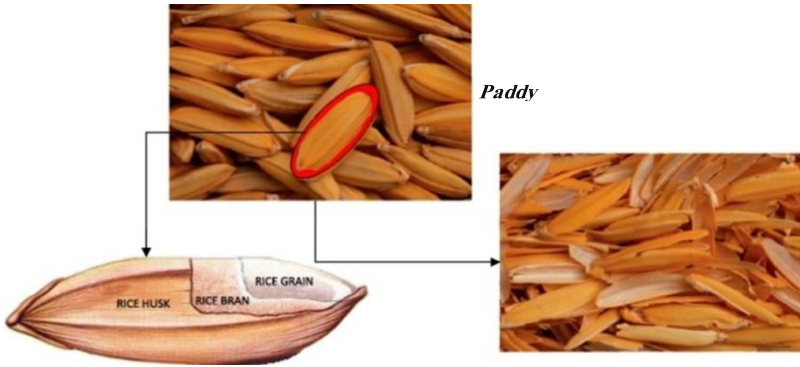


Figure.1.1 Rice grain and respective structures, and rice husk[4].

The hard-protecting rice grain covers known as rice hulls, or rice husks, Figure 1.1 are extracted from rice seed as a byproduct of milling [5]. Rice husk is a valuable raw material that can be used for a variety of purposes. This husk can be added to cement and concrete manufacturing processes or used as a fertilizer in farming. Rice husk's high silicon content has made it a popular source of silica and other silicon compounds, as well as basic silicon preparation. It is well known that rice hulls have a relatively high concentration of inorganic compounds, which make up roughly 20 weight percent of the dry hull and of which silica makes up 94 weight percent. In decreasing concentrations, the remaining (6 weight percent) is made up of K_2O , CaO , MgO , MnO , Al_2O_3 , and P_2O_5 [6]. Cellulose and hemicellulose (50 wt%), lignin (26 wt%), and other organic compounds (four weight percent) make up the majority of the organic compounds (eighty weight percent) in the dry hull. The caryopsis is entirely encased in the two main, modified leaf-like structures known as the lemma and palea that make up rice husk. The smooth outer epidermis with surface hair, where silica is highly concentrated, is the first category of the organized layers of RH [7]. The other three categories are the spongy parenchyma cells, sclerenchyma, and the internal epidermis, which has a relatively soft and hairless surface. Rice husk's vascular bundles are naturally occurring macroporous channels that carry nutrients and water necessary for rice growth. High volatile matter content, almost uniform size, and high ash melting points are characteristics of rice husk [8]. It also contains a comparatively high amount of inorganic compounds, which make up about 26% (wt) of the dry hull. The residual contains 74% (wt) organic compounds. The chemical composition of raw rice husk is listed in table 1-1 [9].

Table 1-1 Chemical analysis of the raw RH.

Constituent	Content (Wt%)
Organic material and moisture	73.87
Al ₂ O ₃	1.23
CaO	1.24
MgO	0.21
MnO	0.074
Fe ₂ O ₃	1.28
SiO ₂	22.12

The percentage of organic compounds in rice husk is 50% (wt) cellulose and hemicellulose, 20% (wt) lignin, and the remaining 3% (wt) is made up of other organic compounds like proteins, oil, and so forth [10]. It is discovered that the chemical makeup of RH varies amongst samples. This variation can be attributed to a number of factors, such as variations in the type of paddy, climatic and geographical conditions, crop year, sample preparation, and analysis technique[11].

1.2 Extraction of silica from rice husk.

Within the other agro-waste family, rice husk ash is one of the raw materials with the highest silica content, containing roughly 90–98% silica (after complete combustion) [12]. For the extraction of silica, simple chemical processes employ non-traditional raw materials, such as rice husk ash, which is heated to high temperatures or extracted using a solvent, sodium silicate, which is extracted from rice husk. The RHA causes structural changes in silica based on the combustion conditions (temperature, time, etc.). Between 550 and 800°C is when amorphous silica forms (Figure. 1.2), while higher temperatures are when

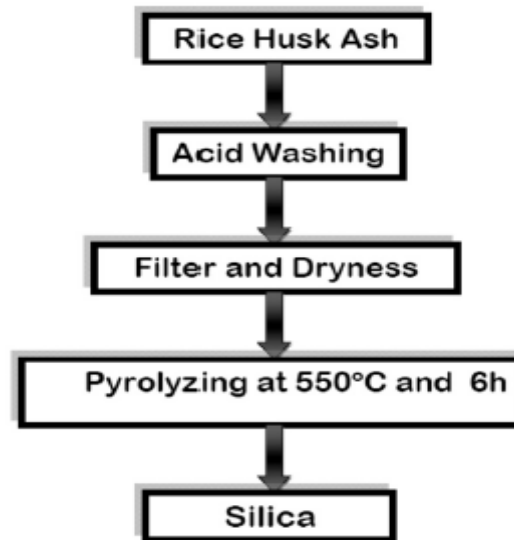


Figure.1.2 Diagram of the procedure was used to extract silica powders from RHA. [13]

Crystalline silica, forms
 Thus, rice husk ash can be utilized to create silicon-based materials of technological interest at a lower cost as a substitute source of amorphous silica [14]. Two million tonnes of high-grade pure silica can be produced using rice husk as the raw material Figure.1.3, meeting the high demands of various industries [15]. In 2009, Prawingwong *et al*, reported employing the sol-gel method to produce mesoporous silica with RHA as the silica source. The resulting silica material has a uniform particle size of 3 nm on average and is amorphous by nature [16].

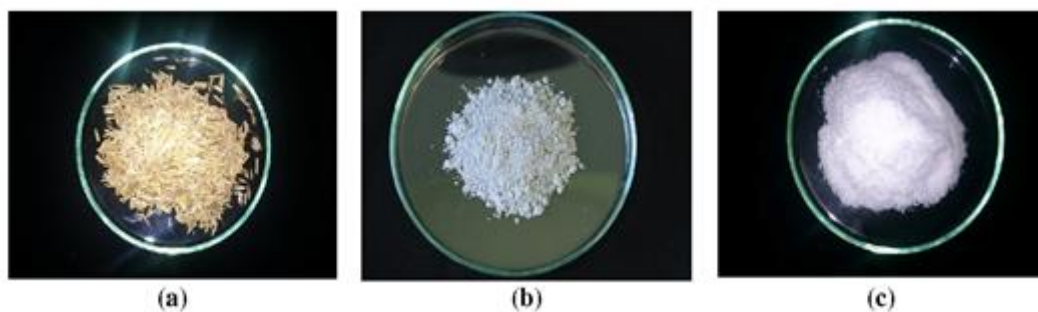


Figure.1.3 (a) rice husk (b) rice husk ash (c) rice husk silica powder [17].

1.3 Silica

Silicon dioxide is the general term for the chemical silica. One silicon atom joined to two oxygen atoms is the chemical formula for this substance, SiO_2 [18]. The compound silica, which is a combination of silicon and oxygen (Figure.1.4), is abundant in the Earth's crust and interior. Over 95% of all known rocks are primarily composed of silica, which also makes up 59% of the crust's mass. Tridymite, cristobalite, and quartz are examples of silica in nature. These silicon dioxide types can be swapped out at the right temperatures [19, 20].

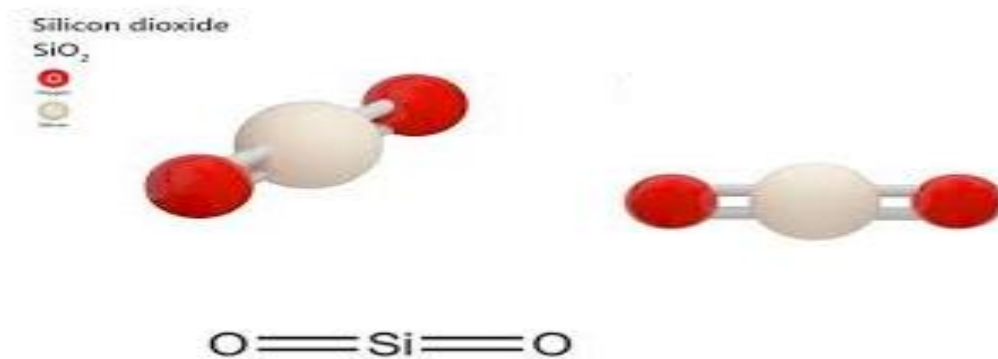


Figure.1.4 Linear structure of silicon dioxide (SiO_2). [21]

Two categories exist for silicon dioxide. One is non-crystalline silica, or amorphous silica. The other is known as crystalline silica. [22]. Covalent bonds bind each silicon atom to four oxygen atoms and each oxygen atom to two silicon atoms in the three-dimensional structure of silicon dioxide. Silicon is surrounded by tetrahedral oxygen atom geometry, as Figure (1.5) illustrates.

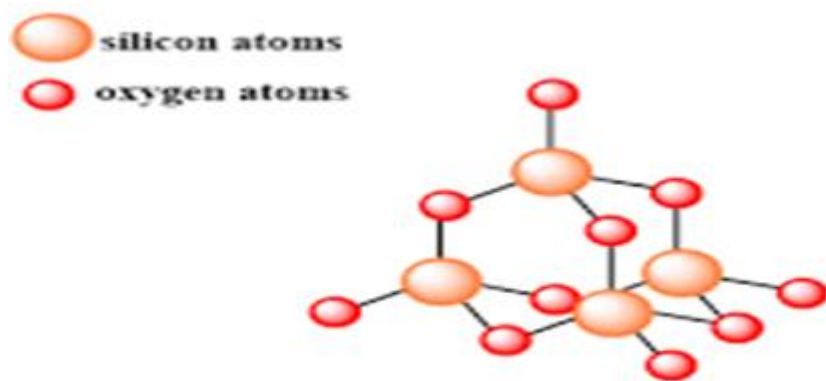


Figure.1.5 crystal structure of silicon dioxide.[23]

Many industries, including food, medicine, electronics, building, and chemicals, use silicon dioxide. Silicon dioxide is a part of drug additives in the pharmaceutical industry[24]. It absorbs moisture and maintains the medication's dryness. Silicon dioxide is utilized in the food industry as an anti-caking agent in spices. It is also used in juices, wines, and beers as a fining agent[25]. In the chemical industry, silicon dioxide finds application in a multitude of production processes. Insecticides, anti-adhesives, adhesives, corrosion inhibitors, dyes, absorbents, sealants, porcelain, and ceramics are also produced using it. In addition, silicon dioxide is used in column chromatography as an absorbent[26]. Curiously, The most common material for optical fibers used in the electronics industry is silicon dioxide. Furthermore, fracturing with silicon dioxide and in the construction industry, hydraulic fracturing is used to produce concrete. Recently, silica, a biosafe component, has been combined with silver nanoparticles to improve the antibacterial and corrosion-resistance of biomaterials. Owing to their large surface area, amorphous silica can be added to thermoplastic polymers. nanoparticles from sources that are natural, such as fly ash and rice husk, can act as a nucleating agent[27, 28].

1-4.Surface of silica

Silica's surface is made up of two different types of functional groups: siloxane (Si–O–Si) and silanol (Si–OH) groups. It was found that a particular molecule's reaction to the silanol groups on the silica surface is the primary modification pathway. On the surface, there are two main processes that generate silanol groups. Initially, during the synthesis of silica, such as during the condensation polymerization of $\text{Si}(\text{OH})_4$, these groups are formed. Second, when water or aqueous solutions are used to treat dehydroxylated silica, surface groups may form as a result of rehydroxylation. Three types of silanol groups on silica surfaces can be distinguished, as shown in Figure.1.6[29]. -Isolated groups (or free silanols) in which the bulk structure of the silicon atom on the surface possesses three bonds, with the fourth bond being attached to a single –OH group [30]. Vicinal silanols (or bridged silanols) where two single groups of silanols connected to distinct silicon atoms are near enough to the hydrogen bond. The two hydroxyl groups that make up geminal silanols are attached to a single silicon atom and are too close to one another to create a hydrogen bond.

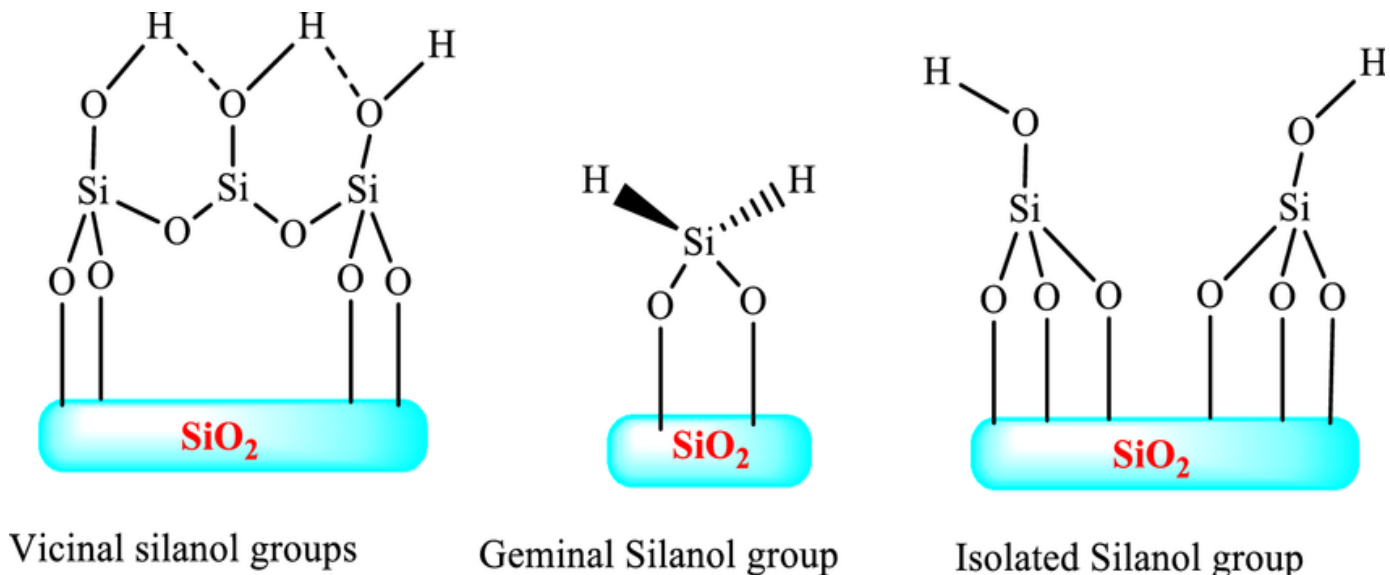


Figure.1.6 Different types of silanol group on the surface of silica.[31]

Conversely, silica exhibits three different kinds of siloxane groups ($\equiv\text{Si}-\text{O}-\text{Si}\equiv$). Figure 1.7 NMR analysis of the ^{29}Si nuclei indicates. [32] Q^n denotes the number of bridging bonds ($-\text{O}-\text{Si}$) that these siloxane groups have attached to the central Si atom. For example, Q^4 denotes four siloxane bonds to the silicon atom, Q^3 denotes three siloxane bonds to the silicon atom, and Q^2 denotes two siloxane bonds to the silicon atom. In general, the following equation can be used to calculate the number of siloxane groups $\text{Si}(\text{OSi})_n(\text{OH})_{4-n} = Q^n$ [33].

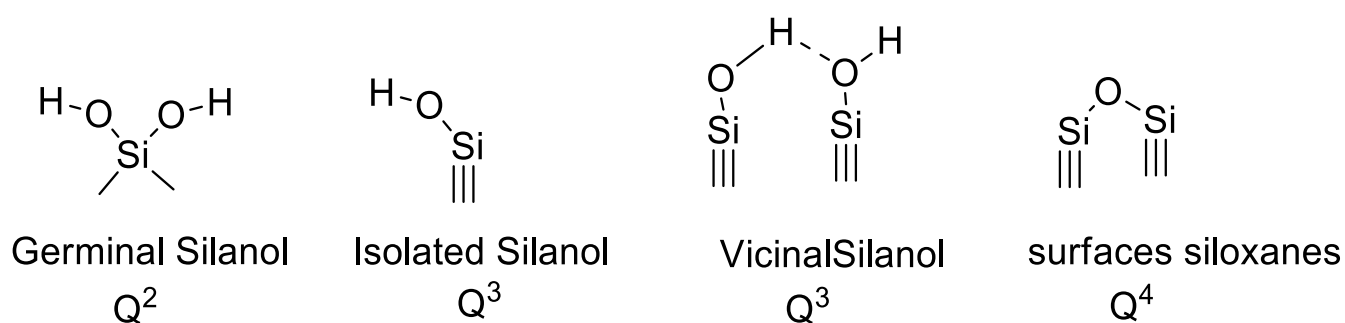


Figure. 1.7 Q^n nomenclature used to define the environment of the silicon atoms in silica.

1-5 Polysiloxane.

Polysiloxanes are polymers with $\sim\text{R}_2\text{SiO}\sim$ repeating units that have variable side groups on the main chain and Si–O bonds with a high bond energy ($\sim 530 \text{ kJ}\cdot\text{mol}^{-1}$) as in the figure (1.8) because of this, they have excellent thermal stability, good gas barrier properties, low dielectric properties, very low surface energy, and excellent biocompatibility. Polysiloxane materials have steadily gained prominence in the chemical, mechanical, electronics, and even aerospace industries since they were first produced commercially in 1940 [34]. The most common polysiloxane structures are linear, cyclic, branching, or three-dimensional. Despite this diversity, controlling the structure and reactivity of silicone-based polymers and materials can be challenging. The process of hydrolyzing or dehydrating chlorosilanes or alkoxy silanes, or the polymerization

of ring-opening compounds facilitated by bases or acids. The siloxane backbone of polymeric silicone materials is typically prepared by -catalyzed ring-opening polymerization of cyclic siloxane monomers, such as cyclotetrasiloxane [35]. These methods, however, are not very suitable for the synthesis of polysiloxanes with precise structural characteristics[36]. Because the chemical nature of Si is similar to that of C as they belong to the same family, silicones have created a semi-inorganic world of their own and were related to the carbon organics but are still destined to be different. Unlike the hydrogen in alkanes, the Si–H groups are hydrides. Its reactivity has led to the emergence of many synthetic methods for controllable polysiloxanes, such as the hydrosilylation reaction. Moreover, the strong Lewis acid catalyst triis(pentafluorophenyl) borane ($\text{B}(\text{C}_6\text{F}_5)_3$; BCF), which was only used in the field of organic synthesis, was found to activate Si–H bonds for many reduction reactions[37]. In the 21st century, with Piers and Rubinsztajn pioneering the application of BCF in the field of catalyzed organosilicon synthesis, the development of structurally controlled polysiloxanes entered a new chapter. The polycondensation reaction between the hydrosilanes, or hydrosiloxanes, and oxygen-based nucleophiles containing -OH groups or alkoxy groups is known as the Piers–Rubinsztajn (PR) reaction, in which BCF activates the Si–H bonds first [13]. An increasing number of applications in areas like metal ion extraction, regeneration, and removal from organic solvents and aqueous solutions are made possible by the addition of chelating groups into polysiloxane matrices [38]. For the extraction and preconcentration of trace metal ions from different media, batch and dynamic techniques frequently employ polysiloxanes functionalized by chelating ligands. As a result, there is an interest in creating functionalized polysiloxanes that have a high potential for absorbing metal ions and the right complexing agents[39].

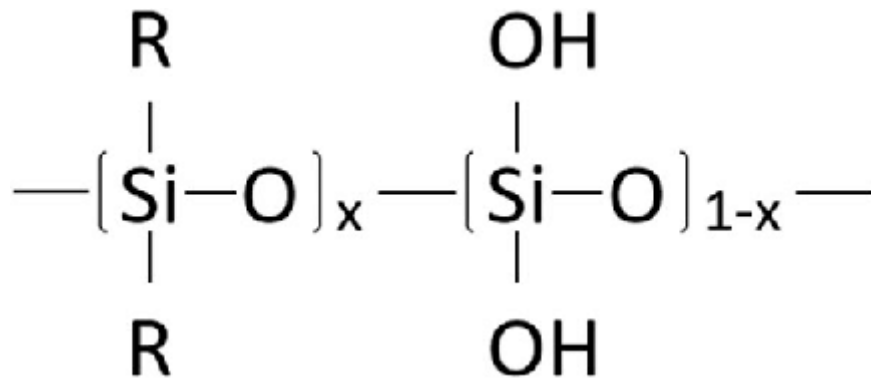
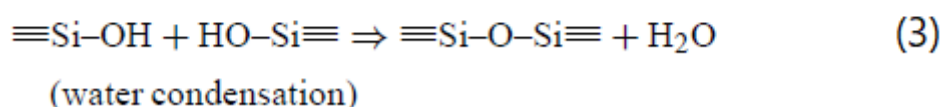
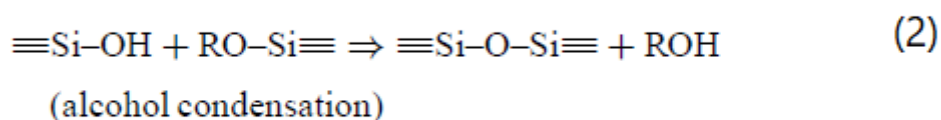
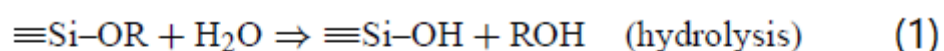


Figure.1.8 Structure of Polysiloxane .[40]

1-6 Sol–Gel Method

Since Dislich developed the sol-gel approaches to make optical coatings of glassy or crystalline systems in 1971, it has been widely used as a way of preparing for single component oxides as well as multiple-component oxides. The term "sol-gel method" refers to the process of creating inorganic polymers or ceramics from solutions by converting liquid precursors into "sols" and then into network structures known as "gels"[41]. Because of its advantages—such as its ability to produce ultrafine particles with a narrow size distribution at room temperatures in a relatively short processing time and its excellent stoichiometric control—the sol-gel method is a useful and appealing technique for the preparation of nano-sized particles. Additionally, it provides a straightforward and straightforward method of synthesizing nano-sized particles, which is essential for nanocatalysts[42]. The two main techniques for obtaining silica particles for sol-gel are top-down and bottom-up approaches. The top-down described by decreasing the size of the initial volume by employing special size[43]. One common route for producing silica nanoparticles at the atomic or molecular scale is the bottom-up or chemical method. Through progressive hydrolysis/condensation reactions from molecular precursors, an amorphous oxide framework is formed as part of the sol-gel process. Metalloid alkoxides, or $M(\text{OR})_n$, are commonly used as precursors[44]. Metal oxide, silica, and organosiloxane matrices with defined porosity and diverse forms could be

produced by sol-gel techniques and used in coatings, sensors, optics, catalysts, and speciality polymers[45]. At room temperature, strong metals or semi-metal oxides can be produced using sol-gel processes that hydrolyze precursors in aqueous solutions. Precursor hydrolysis produces a sol of soluble hydroxylated monomer, which is followed by polymerization and phase separation to form a hydrated oxide hydrogel, as illustrated in below Scheme 1.1. By carefully removing water from the wet gel through extraction or drying, the dry, porous xerogel is created [46].



Scheme 1.1 The suggested reactions of the hydrolysis and condensation processes that occur in the sol-gel method.

There are the three kinds of silica gel are as follows: a) aqua-gel (water fills the pores), b) xerogel (evaporation removes the aqueous phase from the pores), and c) aero-gel (solvent is removed by supercritical extraction)[47]. The synthesis of sol-gel silica starts with liquid precursors, or sol. This process results in the first (wet) gel, where the inorganic network is encircled by solvents. These solvents are then removed to produce a dry material, called xerogel or aerogel(Figure. 1.9) [49].

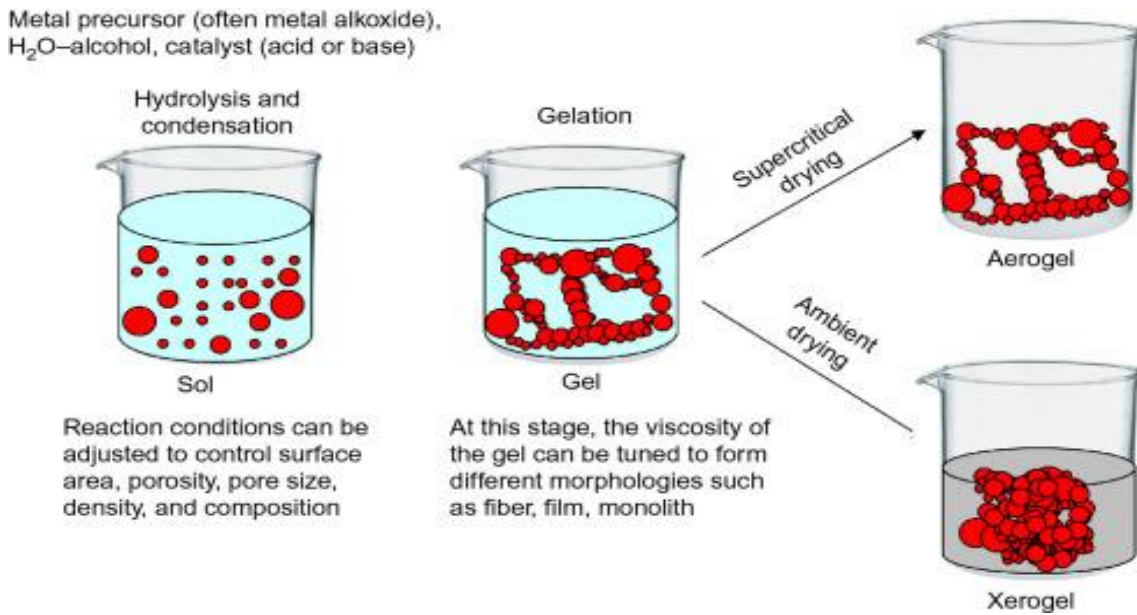


Figure.1.9 Diagram of sol-gel method to yield a dry material (xerogel or aerogel).[48]

Two phases can be distinguished in the composition of silica particles: [49] nucleation and growth. Two models were proposed to define the mechanism of silica growth:[50] regulated aggregation and monomer addition. After an initial burst of nucleation, particle growth occurs, as explained by the monomer addition model. According to the aggregation model, nucleation occurs continuously during the response, and the resulting nuclei (main particles) combine to form larger, dimmer trimmer particles (secondary particles). As shown in Figure. 1.10, both models lead to the formation of a spherical or gel network, depending on the reaction's conditions[51].

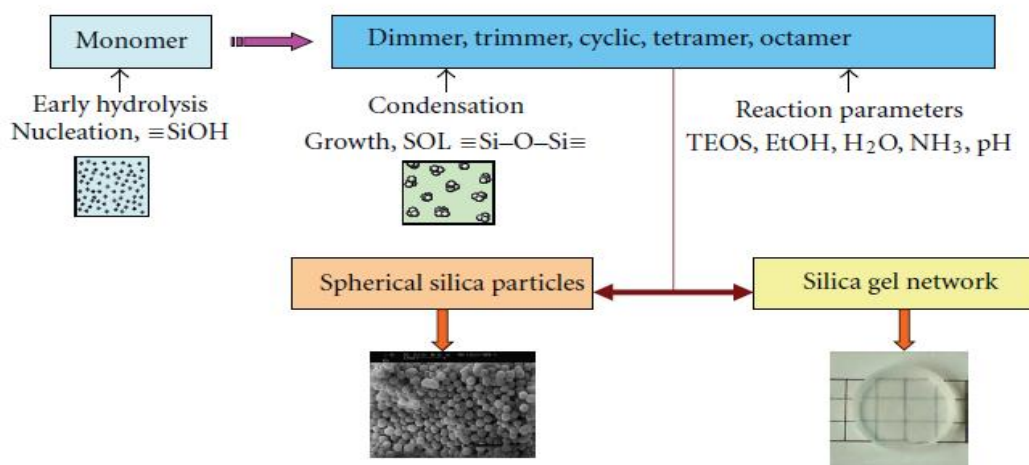


Figure.1.10 Process of sol-gel. [52]

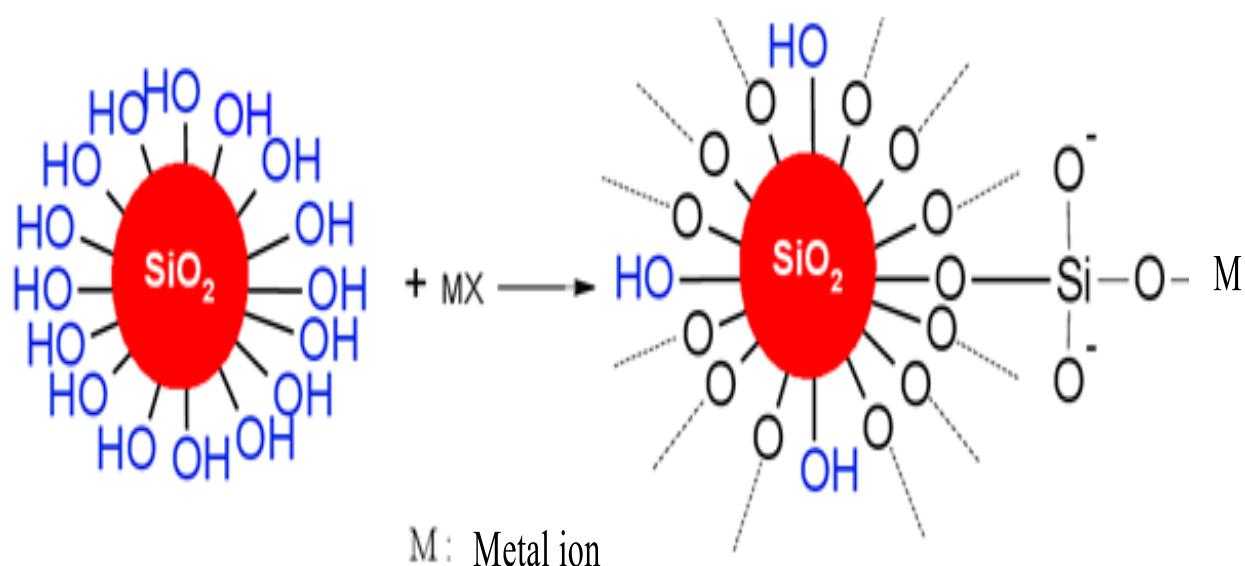
The sol-gel process has a number of advantages over conventional ceramic preparation methods,[53] such as: (1) low reaction temperature; (2) high purity and homogeneity of the products; (3) new and varied compositions; (4) materials with a wide range of shape flexibility; (5) simple reaction systems. (6) Many parameters (such as the amount of water or alcohol, temperature, pressure, type of catalyst, and solvent) can be optimized to control the micro- and macrostructure of the host matrix; (7) the presence of the silica network offers good mechanical resistance, exceptional thermal stability, and an amorphous character; and (8) at low processing temperatures,[54] organic groups can be grafted into the inorganic backbone to produce organic inorganic hybrid materials that are known as ormosils (organically modified silicates),[55] ormolytes (organically modified silicate electrolytes), or ormocers (organically modified ceramics), depending on the final application[56].

1-7 Modification of The Surface of Silica With Metal Ions.

The surface characteristics of silica materials, which are heavily influenced by the superficial functional groups added by various modification techniques, are crucial for their applications[57]. Siloxane (Si-O-Si) and silanol (Si-OH) are the

two types of functional groups that make up the silica surface[58]. As a result, a particular molecule possessing the characteristics of either siloxane (nucleophilic substitution in Si) or silanol (direct reaction with the hydroxyl group) may cause a modification of the silica gel. [59] Nowadays, metal oxide nanoparticles (NPs) have been applied in various fields of nanotechnology including catalysis of chemical reactions, drug delivery, water treatment, textile industries, polymer composites, adhesives, and coatings. The greatest challenge in relation to metal oxide NPs is high tendency to aggregation. Chemical surface modification of metal oxide NPs has gained widely interest to control of dispersion and aggregation of NPs. Silane modifiers are one of the most important bifunctional modifiers that are frequently used for surface treatment of metal oxide NPs. . Then, the recent development in using silane modifiers for treatment of metal oxide NPs in various applications were investigated. It was found that the unmodified NPs have high surface energy and are thermodynamically unstable. Aggregation phenomena is the simple way to reduce the excess surface energy of NPs that leads to an increase in particle size. Therefore, the chemical surface modification of NPs using silanol modifiers can be used as an effective method for the prevention of NPs agglomeration and improvement of NPs stability.[57]

Scheme 1.2, silica surface modification



Scheme 1.2. Silica surface modification.[58]

silanol (Si–O–H) groups at the surface of NPs can interact with the phospholipids of the reticulocyte membranes and lead to hemolysis, for which, surface modification of mesoporous silica nanoparticles (MSNs) by biocompatible polymeric materials such as polyethylene glycol (PEG) would be a perfect solution [59]. For modification of these types of NPs, polymers, metal or metal oxide NPs and antibiotics may be helpful depending on the bacterial species to be targeted. non-porous and MSNs are produced by the microemulsion and Stober's methods, respectively. Other silica NPs, such as hollow MSNs and core-shell silica NPs, may be used to encapsulate and load antibacterial agents. modification of these types of NPs, polymers, metal or metal oxide NPs and antibiotics may be helpful depending on the bacterial species to be targeted [60]. The development of techniques for chemically altering the surface of silica is necessary in order to produce new, highly specific adsorbents, selective heterogeneous catalysts, [61] fillers made of active polymeric materials, and thickeners of dispersive media that work well. For many real-world uses of modified silica, the hydrolytic and chemical stability of surface chemical

compounds is critical.[62] As an example, the following chemical compounds are produced by the reaction between the alcohol and silanol groups[63].



Physical and chemical treatments can be used to modify silica in order to add specific functional groups that will make them suitable for catalytic applications.[64, 65]. Any process that alters the chemical composition of the silica surface is related to surface modification[66]. Surfaces can be altered chemically to change the silica surface's chemical characteristics or physically (heat or hydrothermally) to change the ratio of the silica surface's concentration of silanol and siloxane[67].

Chemical sorption on the silica surface of the active species (i.e., chemical reaction between inorganic/organic species and silanol function) can be used to modify silica gels. Additionally,[68] active species physisorption can be used to modify silica materials, producing a wide range of beneficial supported reagents. Recent years have seen increased research on the application of modified silica gels in trace metal preconcentration. Increased surface fields and improved mechanical stability are advantages of modified silica gels, as demonstrated by applications[69–71].

1.8 Nickel and Copper

Nickel is a chemical element with the symbol Ni and atomic number 28 Figure.1.11. It belongs to the d-level elements and is located at the top of the tenth group elements in the periodic table. Chemically, it is classified as a transition metal. Nickel is a silvery-white metal with a slight golden appearance, and it is a magnetic material. Pure nickel powder has good chemical activity[72]. As for large pieces, they react slowly under standard conditions of pressure and temperature, and this is due to the formation of a passivated layer of oxide on the surface[73]. Nickel is rarely found in nature in its free form, but it is often bound

with other elements within different minerals, especially in ultramafic rock layers. Nickel ores abound in Russia and Canada, as well as on the islands of New Caledonia in the Pacific Ocean.[74] Nickel is produced in the universe from the process of nucleosynthesis in supernovae. It is included in the composition of meteoric iron obtained from iron meteorites, which were widespread on the surface of the Earth in the early historical eras of the Earth's life[75]. Nickel is also included with iron in the composition of the inner and outer core of the Earth.



Figure.1.11 Show the Nickel as element with chemical in formation.[76]

Shen Liu et al. modified nickel with silica surface to prepare nickel-silica nanospheres and hollow nickel nanospheres (Figure. 1.12). Silica nanoparticles were used in the reduction of methylene blue[77].

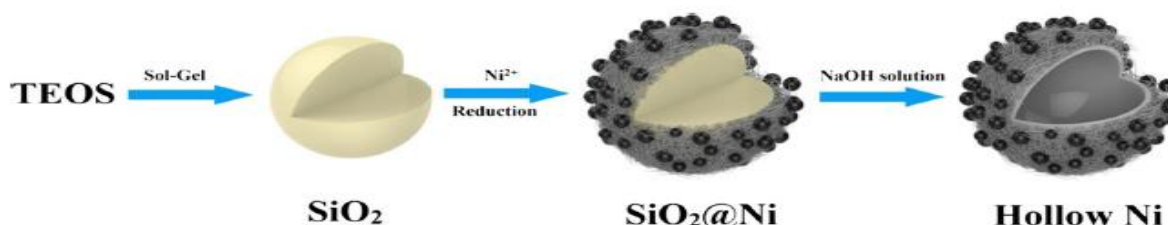


Figure. 1.12 illustration of the synthetic procedure for SiO₂@Ni and hollow Ni microspheres.[77]

Copper is a chemical element with the symbol Cu and atomic number 29 Figure.1.13. It belongs to the d-level elements and is located at the top of the elements of group eleven in the periodic table. Chemically, it is classified as a transition metal. Copper has a distinctive reddish-brown color. It is a soft, malleable metal that is ductile and malleable. It is characterized as a good conductor of electricity and a good transmitter of heat as well[71]. Copper is one of the few metals that can be found in nature in its free form, but it is also included in the composition of a number of minerals in the Earth's crust. Man has known and dealt with copper since ancient history in a number of regions of the world [78–81]. It was the first metal that humans were able to melt and mint into molds, during the historical period between 5000 and 4000 years BC, and that historical era is known as the “Copper Age.” Casting copper with tin led to obtaining the bronze alloy around the year 3500 BC[82] This was also a specific phase in human history, which is referred to as the “Bronze Age.” Copper was mined in ancient Rome mainly from the island of Cyprus, so it is called cuprum in Latin, and from that name the chemical symbol for this element is derived. Copper is used in many applications, such as the manufacture of electrical wires and measuring devices, in the manufacture of alloys, in the minting of coins, in the making of jewellery, and in the decorative arts[83]. Copper has an important biological role, as it is classified as an important mineral element for nutrition. In addition, it is necessary for the functioning of a number of enzymes, such as the enzyme cytochrome c oxidase, which is important for cell respiration. Copper is also a component of hemocyanin, which is the hemoglobin in some living organisms like molluscs and crustaceans. On average, humans contain between 1.5 and 2 milligrams of copper per kilogram of body weight, and it is concentrated in the liver, muscles, and bones[83].



Figure.1.13 Show the Copper as Element with Chemical in formation.[84]

1-9 Biological Activity of (Metals-Silica) Materials

Nanomaterials have been used as therapeutic agents as alternative compounds for drugs, as they act as antimicrobials such as fungi and bacteria. Another reason is that many bacterial strains have the ability to adhere to any natural surface and form a biofilm to protect them from external factors. Therefore, nanomaterials act as antimicrobial agents by reducing bacterial adhesion and biofilm formation, as they inhibit bacterial protein formation by binding to bacterial ribosomes. It has been proven that the compounds (NPs Ni and NPCu) interact with DNA Figures.1.14 & 1.15, which leads to their work as an antimicrobial, as microbial cells absorb the compounds (Ni-SiO and Cu-SiO divalent and reduced) by the electromagnetic force present on the surface of these compounds, and silver ions Ni, Cu are released from the NPs Ni, NPCu compounds and transferred to the cytoplasm[85].

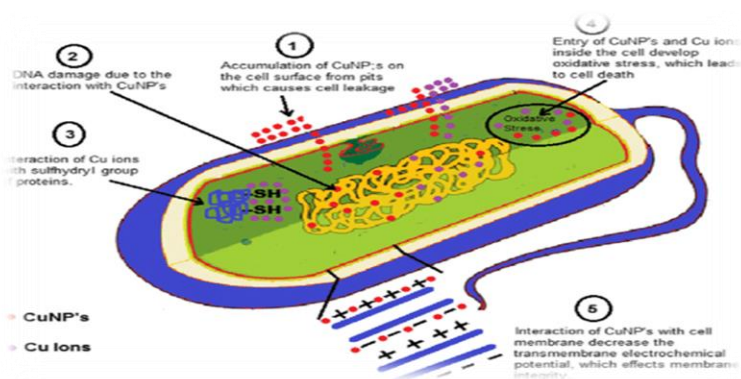


Figure.1.14 Mechanism for antibacterial activity of copper nanoparticles.[86]

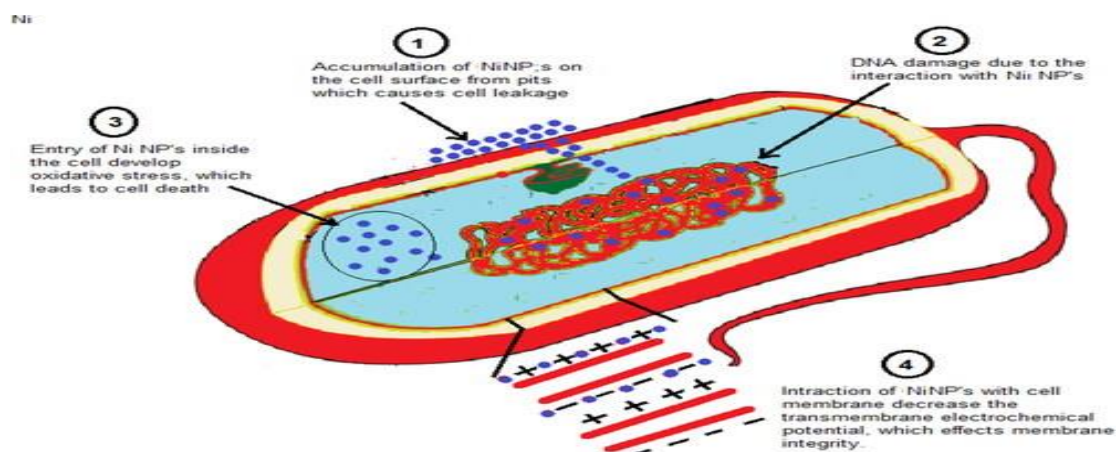


Figure 1.15 Different possible mechanisms associated with the antimicrobial activity of Ni(0)/NiO NPs.[87]

Nickel and copper ions interact directly with mitochondria inside the microbial cell, which leads to the formation and generation of Ros and thus inhibiting DNA replication. In particular, nickel and copper nanoparticles wide applications through their work as antivirals, antifungals and antibacterial agents that cause various diseases Broad spectrum antimicrobial against a wide range of microorganism[88].Every day, billions of microorganisms interact with the human body. Thirty percent of microorganisms are harmful. They have the potential to affect human health, but the majority are beneficial and symbiotic. Therefore, fresh approaches getting rid of those infections are required. The creation of novel materials with long half-lives, neutral environmental effects, and antibacterial or antifungal qualities is one of the relatively new ideas for preventing pathogens. Metallic nanoparticles (NPs), particularly those of silver, copper, zinc, or nickel, are one possible remedy[85]. Their antimicrobial activity is caused by damage to DNA and the cell membrane. Interaction with thiol group-containing enzymes are connected to the production of hydrogen peroxide. Furthermore, the particle size, agglomeration, or release rate of metal ions all have a significant impact on the biotical qualities of metallic nanoparticles. They

are thought to have less effect on the environment than organic compounds. Thus, metallic nanoparticles are added to everyday organic and inorganic products like pesticides, detergents, protective wood finishes, cosmetics, and dietary supplements. Because of how simple it is for metal ions to leak into the environment, there are certain restrictions on the use of metallic nanoparticles. Moreover, nanoparticles can move from products into water and subsequently infiltrate ecosystems through sewage. Metals can therefore readily accumulate in soil and be absorbed by plants, then make their way up the food chain. Moreover, it is impossible to fully distinguish between the harmful effects of nickel and copper ions and nanoparticles. According to recent research by Y Springer Wu, L Kong *et al.*, they must be combined with proteins and silica to inhibit the production of Ni(II) ions and lessen their toxicity [89]. Alternatively, metal nanoparticles can be packed into an organic or inorganic matrix, such as a polymer, ceramic, or glass, to create nanocomposite coatings. It has been shown that the antibacterial and biomedical properties can be improved by combining metal nanoparticles with magnetite (Fe₃O₄) or water-soluble polymer (PEG) nanoparticles and nickel nanoparticles of suitable sizes (<100 nm) prepared as coatings. However, the most adaptable matrices appear to be made from chemically modified silica. Metal ions embedded in a silica matrix have been shown to have a wide range of potential applications; in particular, they can be used as cytotoxic agents against fungi and bacteria in copper- and silver-based systems[90]. The nanoparticle system and silica (Cu, Ag, Ni/SiO₂) showed, according to the study conducted by the researcher Huda *et al.* on the biological effectiveness of elements doped on silica, that elements doped on silica have high biological effectiveness against fungi[87]. It is important to note that the manufacturing processes used to create these Nano composites - such as chemical reactions, sol-gel or spray deposition - often have a significant impact on their effectiveness. The unique physical and chemical properties of nanomaterials, along with their potential biomedical applications, have sparked intense research

worldwide[91]. Synthetic pathways to a variety of nanoparticles with varied compositions and properties and a wide range of chemical and biological applications have been developed over the past 20 years. Despite their high cost, noble metals from gold and silver are used in the synthesis of NPs. Therefore, copper (Cu) and nickel (Ni) are good alternative materials, in this situation [92]. Other metals that may have antibacterial properties, like Cu and Ni, have also been the subject of recent research. Although some studies have already demonstrated certain characteristics of alloy NPs that set them apart from pure ones, little attention has been given to the study of bimetallic Cu–Ni NPs Cu NPs and as well as copper oxide NPs and have already been shown to possess antimicrobial properties. For Ni NPs, similar results have been reported ;Nevertheless, there aren't many studies on this subject. Research has demonstrated the bactericidal activity of Cu and Ni NPs. However, stabilizers like polymers, ligands, salts, etc. that can impair their qualities have been used to synthesize them in aqueous solution. [93][87]. Thus, the synthesis and characterization of Cu, Ni, and bimetallic Cu–Ni NPs as well as an investigation into their antimicrobial activity. Copper and its complexes have been used for centuries as disinfectants due to their antibacterial as well as antiviral properties . It is believed that the enhanced antimicrobial activity of Cu-NPs compared to copper salts is due to their large surface to volume ratio and crystallographic surface structure. Currently, the search of new antibacterial agents is particularly important because of the gradual increase of new bacterial strains resistant to the most potent antibiotics.[94]. Recently, nickel nanoparticles (NiNPs) have gained a lot of attention because of their promising qualities, which include high reactivity, an excellent surface area to volume ratio, and an environmentally friendly or nontoxic nature. In a variety of industrial and medicinal applications, NiNPs' catalytic, photocatalytic, antibacterial, antifungal, electrochemical, and antioxidant qualities are useful[95–97]

1-10 The Aims.

- 1.Preparation of sodium silicate from Rice Husks.
- 2.Preparation of silica- metal(nickel and copper) nanoparticles using sol-gel method.
- 3-Characterizations of preparing samples by FT-IR, XRD, FE SEM-EDX , X-ray photoelectron (XPS),N₂- adsorption- desorption, AFM, TEM, TGA/DTA,BET, UV–Vis (DRUV–Vis) and ICP-MS.
- 4-Possibility of applying the nanoparticles as antimicrobial agents.

CHAPTER TWO

EXPERIMENTAL PART

2.Experimental Part

2.1 Instruments

Table 2-1: List of instruments, supplier companies and place of measurement.

Instrument	Manufacturer	Place of measurement
FTIR	Shimadzu 8400s	Beam Gostar Taban Lab/Iran
UV-Vis	Shimadzu double beam 1800 UV	Beam Gostar Taban Lab/Iran
XRD	Shimadzu X-ray Diffractometer	Beam Gostar Taban Lab/Iran
SEM-EDX	FESEM MIRA III (TESCAN)	Beam Gostar Taban Lab/Iran
BET	BEL BELSORP MINIII	Beam Gostar Taban Lab/Iran
TGA/DTA	SDT Q600 V20.9 Build 20	Beam Gostar Taban Lab/Iran
XPS	Eager 300 for EA1112	Beam Gostar Taban Lab/Iran
Water bath	Lab. Companion BS-11 shaking water	University of Kerbala / College of science – Iraq
Oven	Model un 110 plus	University of Kerbala / College of science – Iraq
Hot plate magnetic stirrer	LMS1003, Labtech, Techco, LTD	University of Kerbala / College of science – Iraq
TEM	Philips CM12	Beam Gostar Taban Lab/Iran
AFM	CSPM-AA3000	Beam Gostar Taban Lab/Iran
ICP	Xiamen Dexing Magnet Tech. Co., Ltd	Beam Gostar Taban Lab/Iran

2.2. Materials

All chemicals were used directly without further purification. Rice husks were collected from a local factory for rice production in Najaf Governorate-Abbasiya city. Table 2-2 shows the chemicals used in this work.

Table 2-2 Chemicals used in this work and their provider.

Chemical	Formula	Purity (%)	Provider
Acetone	C ₃ H ₆ O	98	ROML British
Nickel Nitrate hex hydrate	Ni(NO ₃) ₂ .6H ₂ O	89	GCC, England
Ethanol	C ₂ H ₅ OH	99	Sigma-Aldrich, Germany
Copper Nitrate tri hydrate	Cu(NO ₃) ₂ .3H ₂ O	99	Merk, KGaA, Germany
Sodium Brohydride	NaBH ₄	99	Sigma-Aldrich, Germany
Nitric acid	HNO ₃	70	CDH, India
Sodium hydroxide	NaOH	96	BDH, England
DMSO	Di methyl sulfoxide	95	ROML British

2.3 The Preparation Methods:

2.3.1 Preparation of Sodium Silicate Solution From Rice Husks

The crud rice husk (RH) washed with distilled water to remove dirt and other contaminants present was it, and then was dried at room temperature for 24 hours. Approximately 30.0 g of cleaned and dried rice husks were weighed and transferred to a plastic container. HNO₃ (500 mL , 1.0 M) was added into the

container and stirred for 24 hours in order to remove unwanted metal oxides such as Al_2O_3 , Na_2O , K_2O , CaO , MgO , MnO and Fe_2O_3 . Then the acid-soaked rice husk were filtered, washed with copious amounts of distilled water, dried at 100°C for 24 hours and marked with the symbol RH- NO_3 . About 30.0 g of cleaned, dried and nitric acid treated rice husks were weighed and transferred into a plastic container. sodium hydroxide (500 mL , 1.0 M) was added to the container and stirred for 24 h to prepare sodium silicate [55, 98]. Then the cellulose was removed as solid and the silicate solution was taken as raw material to prepare the required materials in the subsequent steps.

2.3.2 Preparation of Nickel Silica Nanoparticles $\text{SiO}_2@\text{Ni(II)}$.

HNO_3 (50ml,3M) containing 10 wt.% of $\text{Ni}(\text{NO}_3)_2 \cdot 6\text{H}_2\text{O}$ was added slowly to the solution of sodium silicate prepared in the above paragraph. The gel began to appear at pH 10 and formed 5.5. The resulting solution containing the light brown gel was set aside for 24 hr. Following gel aging, the mixture was subjected to centrifugation using a Hettich centrifuge at a speed of 4000 revolutions per minute. Subsequently, the gel was filtered, completely rinsed with distilled water, and ultimately dried in an oven at a temperature of 110°C . The material was chilled in a desiccator and kept in a tightly sealed container for analysis and further use as an antibacterial agent. The chemical symbol given to this specimen was $\text{SiO}_2@\text{Ni(II)}$. The schematic diagram illustrating the procedure for synthesizing $\text{SiO}_2@\text{Ni(II)}$ from rice husk is shown in Scheme 2.1.

2.3.3 Preparation of Reduced Nickel Silica Nanoparticles $\text{SiO}_2@\text{Ni(0)}$.

One and a half gram of nickel-silica nanoparticles ($\text{SiO}_2@\text{Ni(II)}$) was dissolved in 50 mL of cold deionized water, and a suspension solution of nickel-silica nanoparticles was obtained. Then, an excess of NaBH_4 as a reducing agent (2.0 g) was added and then stirred vigorously in an ice bath for three hours; during this

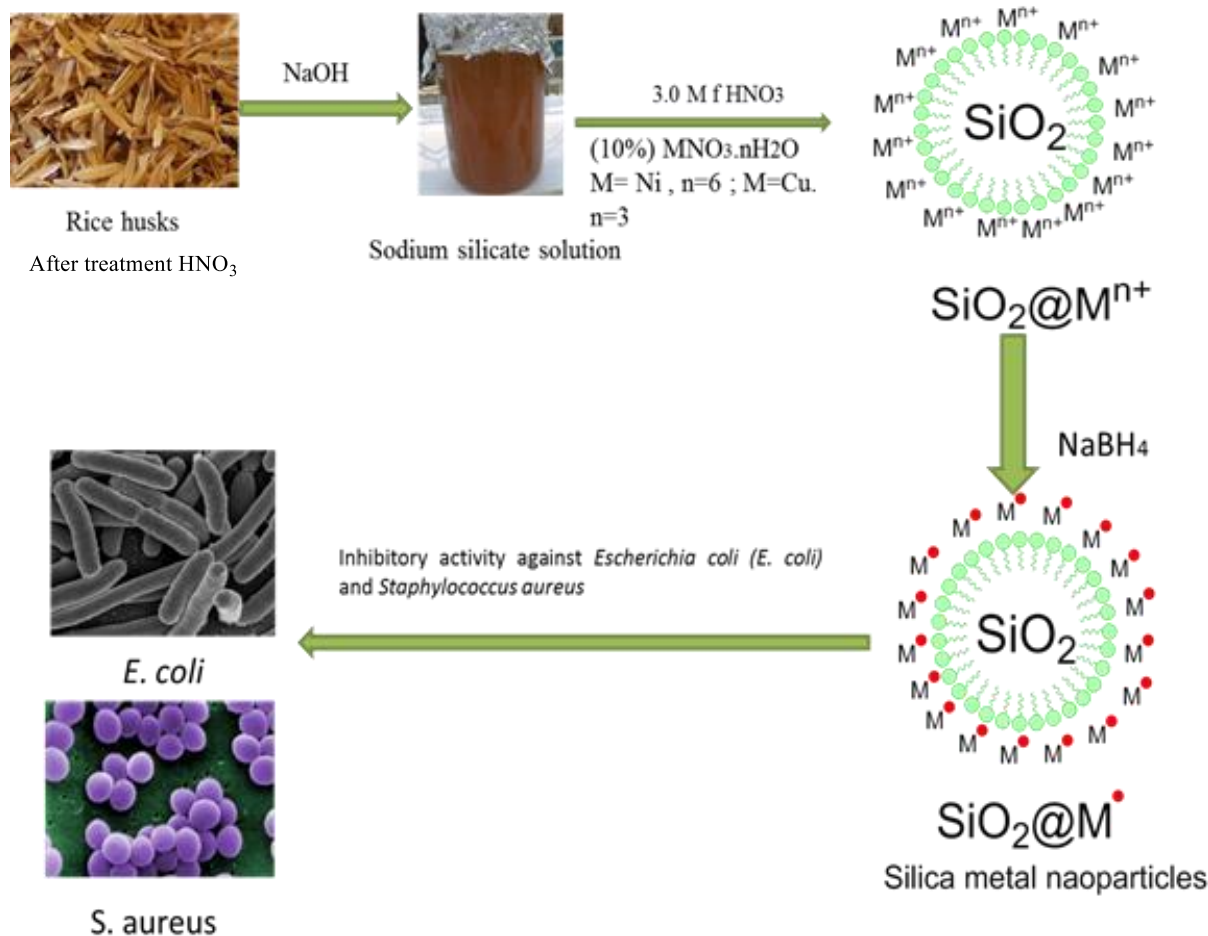
time, the color of the suspension was changed to light green. After that, a colored precipitate was obtained, filtered, washed with deionized water several times, and placed in the oven at 110 °C for 24 h. After cooling, 1.3 g of the final product was obtained, labeled as $\text{SiO}_2@\text{Ni}(0)$, and placed in the desiccator to be characterized by appropriate physical measurements. A schematic diagram of the method for preparing $\text{SiO}_2@\text{Ni}(0)$ is shown in Scheme 2.1.

2.3.4 Preparation of Copper Silica Nanoparticles $\text{SiO}_2@\text{Cu(II)}$.

Fifty millilitres of 3 M HNO_3 containing 10 wt.% of $\text{Cu}(\text{NO}_3)_2 \cdot 3\text{H}_2\text{O}$ was added slowly to the (200 mL) solution of sodium silicate. The gel began to appear at pH 10 and reached 5.5. The resulting solution containing the dark nutty gel was set aside for 24 hr. Following gel aging, the mixture was subjected to centrifugation using a Hettich centrifuge at a speed of 4000 revolutions per minute. Subsequently, the solution was filtered, completely rinsed with distilled water, and ultimately dried in an oven at a temperature of 110 °C. The material was chilled in a desiccator and kept in a tightly sealed container for analysis and further use as an antibacterial agent. The chemical symbol given to this specimen was $\text{SiO}_2@\text{Cu(II)}$. The schematic diagram illustrating the procedure for synthesizing $\text{SiO}_2@\text{Cu(II)}$ from rice husk is shown in Scheme 2.1.

2.3.5 Preparation of Copper Silica Nanoparticles $\text{SiO}_2@\text{Cu(0)}$.

One gram of copper -silica nanoparticles ($\text{SiO}_2@\text{Cu(II)}$) was dissolved in 50 mL of cold deionized water, and a suspension solution of copper-silica nanoparticles was obtained. Then, an excess of NaBH_4 as a reducing agent (2.0 g) was added and then stirred vigorously in an ice bath for three hours; during this time, the color of the suspension was changed from dark nutty to light olive. After that, a colored precipitate was obtained, filtered, washed with deionized water several times, and placed in the oven at 110 °C for 24 h. After cooling, 0.9 g of the final product was obtained, labeled as $\text{SiO}_2@\text{Cu(0)}$. A schematic diagram of the method for preparing $\text{SiO}_2@\text{Cu(0)}$ is shown in Scheme 2.1.



Scheme.2.1 Preparation of nickel-silica nanoparticles SiO₂@Ni(II), SiO₂@Ni(0) and copper-silica nanoparticles SiO₂@Cu(II),SiO₂@Cu(0) from rice husk

2.3.6 Antimicrobial Assay

2.3.6.1 Bacterial Isolate

Escherichia coli (*E. coli*) and *Staphylococcus aureus* (*S.aureus*) were received from the Al-Husseini Teaching Hospital in Holly Karbala. These strains were biochemically diagnosed using an API staph system applied according to the manufacturer's instructions .

2.3.6. 2Antibacterial Activity of Silica Nanoparticles

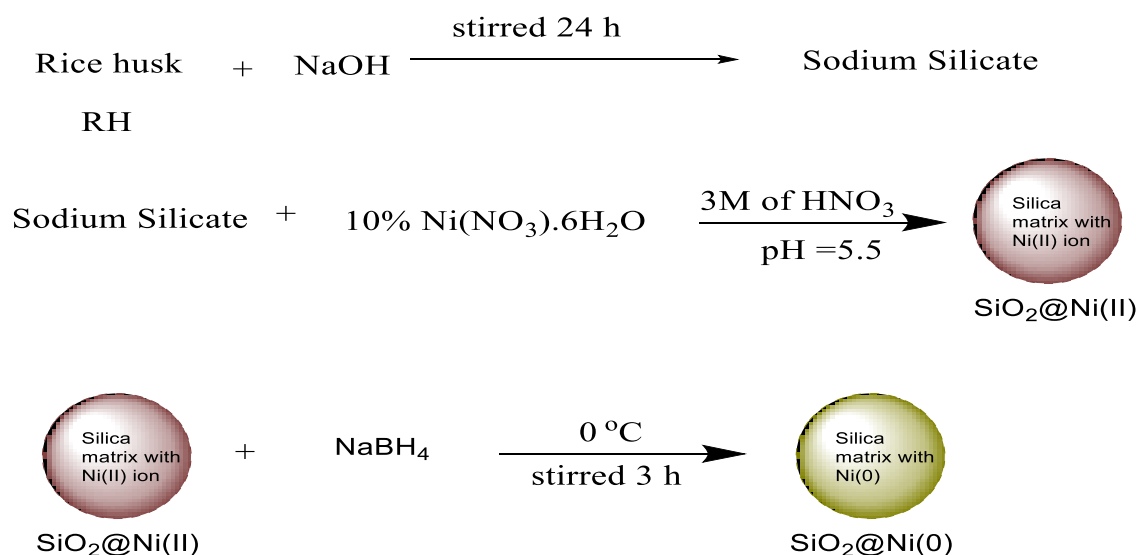
The bacterial number of the studied strains *E. coli* and *S. aureus* suspensions were controlled by comparing their density to the 0.5 McFarland tube (108 CFU/mL) as a standard suspension. The serial dilutions (20-100 mg/mL) of SiO₂@Ni(II), SiO₂@Ni(0), SiO₂@Cu(II) and SiO₂@Cu(0) were prepared, and then strains under investigation were cultivated on muller-Hinton agar. Holes with a diameter of 8 mm were created using a cork borer, and each hole was properly filled with 100 µL of each chemical concentration using micropipettes. Additionally, one hole was filled with DMSO as a negative control. Subsequently, the Petri plates were placed in an incubator set at a temperature of 37 degrees Celsius for a duration of 24 h. Following the incubation period, the observation of each plate was conducted, and the measurement of the inhibition zone was performed using a ruler. This process was done three times for each concentration. The minimum inhibitory concentration (MIC) of the compound was determined as the lowest concentration of a studied substance that killed all bacterial cells or in which no bacterial growth was seen [99].

CHAPTER THREE

RESULTS AND DISCUSSION

3.1 Synthesis and Characterization of SiO₂@Ni(II) and SiO₂@Ni(0)

To the solution of sodium silicate, 3 M HNO₃ containing 10 wt.% of Ni(NO₃)₂.6H₂O was added. The appearance of the gel began at pH 10 until reached 5.5. A sufficient. The resulting solution containing the light brown gel was set aside for 24 hr. After aging. The gel separated by centrifugation using a Hettich centrifuge at a speed of 4000 revolutions per minute. After that dried in an oven at a temperature of 110 °C and labeled as SiO₂@Ni(II). About 1.5 g of SiO₂@Ni(II) was dissolved in 50 mL of cold deionized water, Then, an excess of NaBH₄ as a reducing agent (2.0 g) was added and then stirred vigorously in an ice bath for three hours; during this time, the color of the suspension was changed to light olive. After that, a colored precipitate was obtained, filtered, washed with deionized water several times, and placed in the oven at 110 °C for a whole day. After cooling it, 1.3 g of the final product was obtained, labeled as SiO₂@Ni(0). A schematic diagram of the method for preparing SiO₂@Ni(II) and SiO₂@Ni(0) is shown in Scheme 3.1.



Scheme 3.1 Preparation of SiO₂@Ni(II) and SiO₂@Ni(0) from rice husk

3.1.1 Fourier Transform Infrared Spectroscopy (FTIR)

The synthesized nickel-Silica nanoparticles $\text{SiO}_2@\text{Ni(II)}$ and $\text{SiO}_2@\text{Ni(0)}$ were characterized using FTIR spectroscopy (Figure. 3.1). The spectra of $\text{SiO}_2@\text{Ni(II)}$ and $\text{SiO}_2@\text{Ni(0)}$ showed the typical absorption bands around 3430 cm^{-1} , which are assigned to stretching vibrations of silanol (Si-OH) and stretching vibrations of physically absorbed water with silica [55, 100, 101]. The absorption bands around 1630 cm^{-1} are ascribed to the bending vibrations of absorbed water with the silica surface[6, 102]. The absorption bands around 800 cm^{-1} and $1100\text{--}1020\text{ cm}^{-1}$ are ascribed to the symmetric and antisymmetric stretching vibrations of the siloxane group (Si-O-Si), respectively[103, 104]. The stretching vibrations of Ni-O-Si appeared around (700 cm^{-1}) [105, 106], and it was noted that it disappeared in $\text{SiO}_2@\text{Ni(0)}$ due to the reduction of Ni(II) to Ni(0) . The actual locations of all peaks are shown in Figure.3.1.

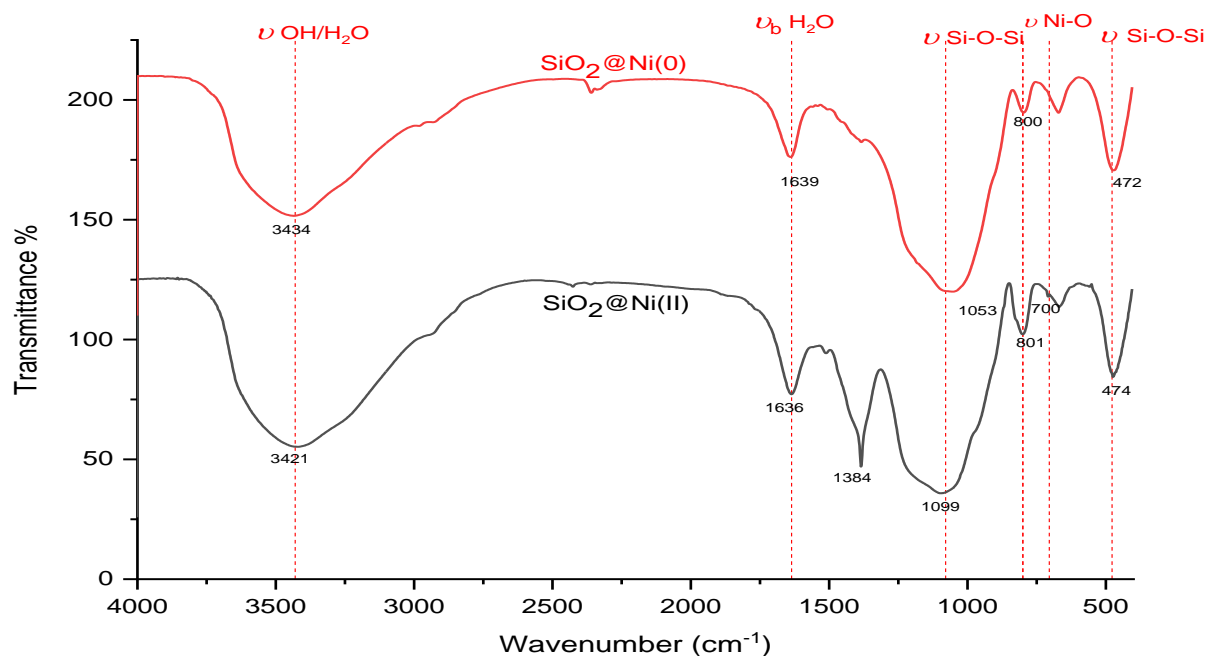


Figure. 3.1 FTIR spectra of $\text{SiO}_2@\text{Ni(II)}$ and $\text{SiO}_2@\text{Ni(0)}$

3.1.2 X-Ray Diffraction Analysis (XRD)

Figure.3.2 shows the XRD patterns of nickel-modified silica particles $\text{SiO}_2@\text{Ni(II)}$ and $\text{SiO}_2@\text{Ni(0)}$. In both patterns, a broad peak between 15 and 30 of 2θ is observed, which is characteristic of amorphous silica[32, 107]. The sharp peaks characteristic of nickel oxide are not observed, but instead, broad peaks of nickel metal are observed at $2\theta = 35^\circ$, 47° and 60° which show the weak crystal structure of $\text{SiO}_2@\text{Ni(II)}$ and $\text{SiO}_2@\text{Ni(0)}$. These results are consistent with other references[108–110].

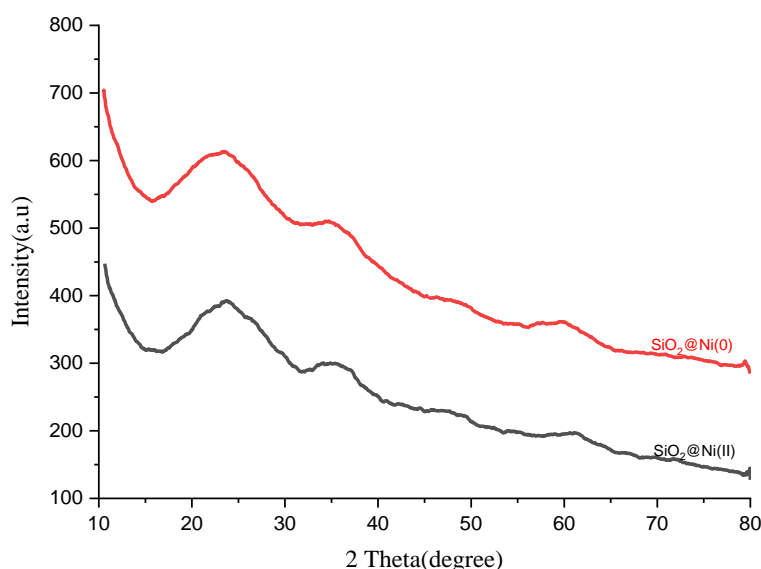


Figure. 3.2 The XRD pattern of $\text{SiO}_2@\text{Ni(II)}$ and $\text{SiO}_2@\text{Ni(0)}$

3.1.3 N_2 Adsorption–Desorption Analysis

The physical properties of nickel-silica particles $\text{SiO}_2@\text{Ni(II)}$ and $\text{SiO}_2@\text{Ni(0)}$ were studied using the N_2 - adsorption/desorption technique, as shown in Figures. 3.3 A&B, respectively. Observing Fig.3.3 of isotherms and their hysteresis loops reveals the IV type [107, 111, 112] and the hysteresis type is H3 [98, 113], which belongs to mesoporous materials where the interactions between gas molecules

and adsorbent mesopore surface lead to capillary condensation. The inset in Fig.3.3 shows the corresponding pore size distribution for both materials $\text{SiO}_2@\text{Ni(II)}$ and $\text{SiO}_2@\text{Ni(0)}$, as the pore distribution falls within the range of 2-10 nm, which falls in the mesoporous range. Table 3.1 shows the result of the N_2 -adsorption/desorption analysis of $\text{SiO}_2@\text{Ni(II)}$ and $\text{SiO}_2@\text{Ni(0)}$.

Table 3-1 The result of N_2 - adsorption/desorption analysis of $\text{SiO}_2@\text{Ni(II)}$ and $\text{SiO}_2@\text{Ni(0)}$

Compound	Specific surface area(m^2/g)	Average pore volume ($\text{cm}^3 \text{g}^{-1}$)	Mean pore diameter (nm)
$\text{SiO}_2@\text{Ni(II)}$	108.720	0.339	12.502
$\text{SiO}_2@\text{Ni(0)}$	99.538	0.336	13.508

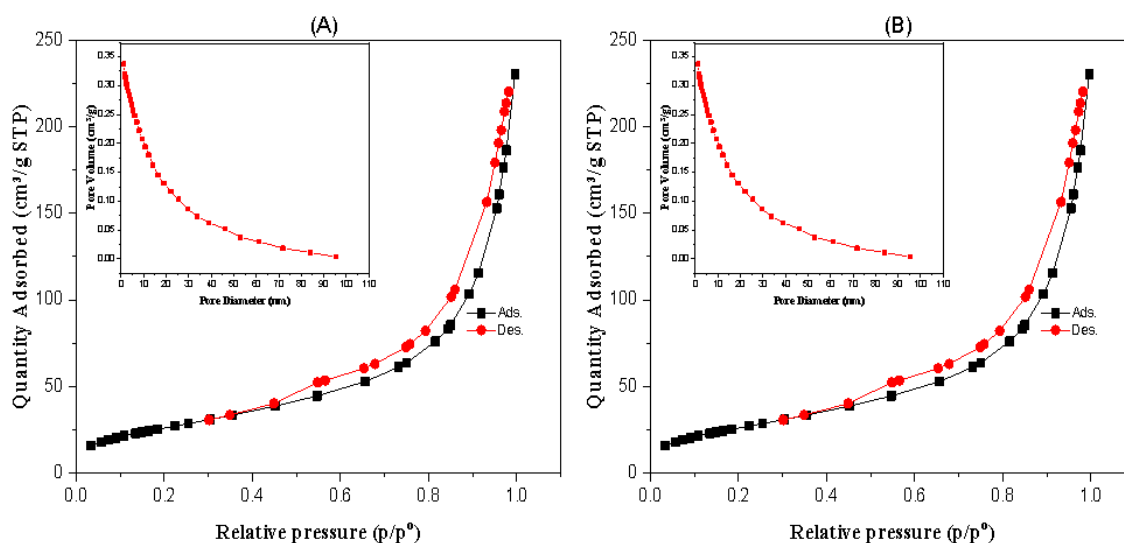


Figure. 3.3 The nitrogen adsorption–desorption isotherms of (A) $\text{SiO}_2@\text{Ni(II)}$ and (B) $\text{SiO}_2@\text{Ni(0)}$. The inset shows the corresponding pore size distribution.

3.1.4 Field Emission Scanning Electron Microscopy (FESEM) Analysis

The morphological characteristics of silica compounds modified with nickel $\text{SiO}_2@\text{Ni(II)}$ and $\text{SiO}_2@\text{Ni(0)}$ were studied by field emission scanning electron microscopy (FESEM) analysis. FESEM analysis of the prepared composites

showed uniform shape and spherical particle morphology (Figure.3.4 A&C). The average size of modified silica was (50-150) nm between the mesoporous and macroporous ranges [77, 114] It is worth noting that the $\text{SiO}_2@\text{Ni}(0)$ particles are more regular and spherical than $\text{SiO}_2@\text{Ni}(\text{II})$. The EDX spectra of $\text{SiO}_2@\text{Ni}(\text{II})$ and $\text{SiO}_2@\text{Ni}(0)$ in Fig.3.4 B&D shows the presence of the basic elements in the sample, which are silicon and oxygen, in addition to the presence of nickel particles. This can be considered supportive evidence for the success of the process of preparing nickel-supported silica particles.

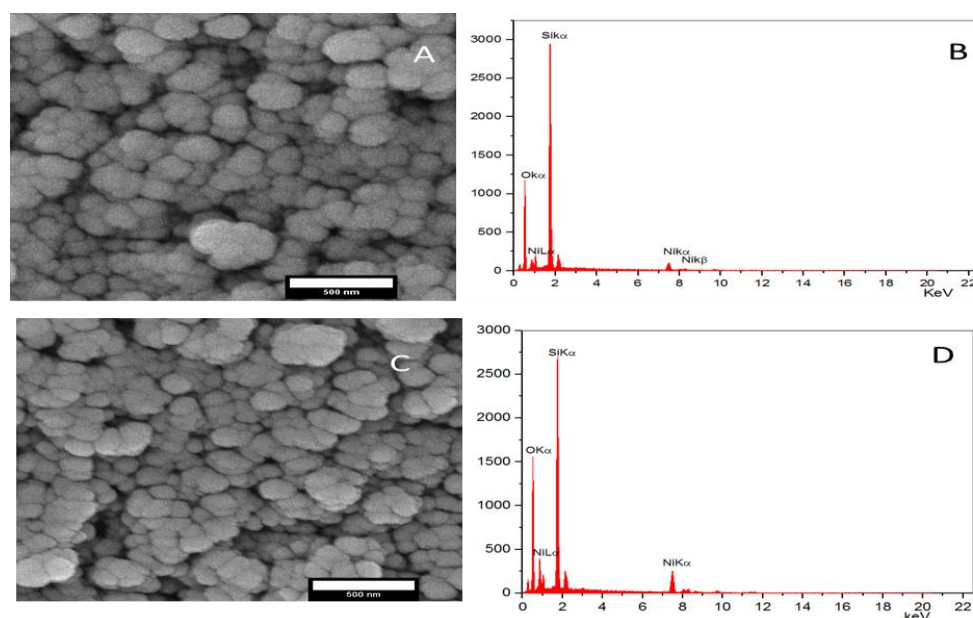


Figure. 3.4 A & B FESEM-EDX for $\text{SiO}_2@\text{Ni}(\text{II})$, C & D FESEM-EDX for $\text{SiO}_2@\text{Ni}(0)$

3.1.5 Transmission Electron Microscopy (TEM) analysis

TEM image of compounds $\text{SiO}_2@\text{Ni}(\text{II})$ and $\text{SiO}_2@\text{Ni}(0)$ in figure 3.5 are displayed that nickel-silica nanoparticles contain some random pores in an irregular, heterogeneous, and interconnected shape, with a diameter ranging between 15-20 nm. This indicates that the nickel-silica nanoparticles have a mesoporous nature. The images also showed dark black spots that could be attributed to nickel oxides.

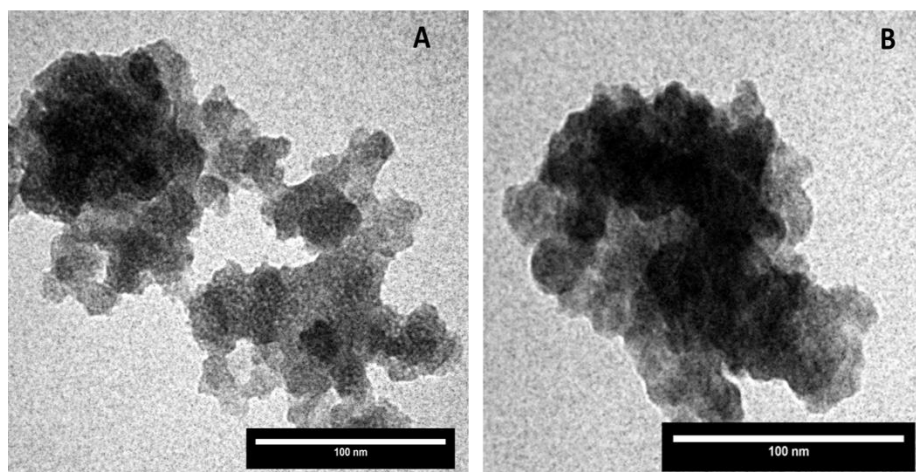


Figure.3.5 A The TEM image of $\text{SiO}_2@\text{Ni(II)}$ and B The TEM image of $\text{SiO}_2@\text{Ni(0)}$

3.1.6 Atomic Force Microscopy (AFM)

Atomic force microscopy (AFM) is an influential surface analysis technique used to study the topography of silica nanoparticles. This technique can be used to obtain high-resolution 2D and 3D nano images and to study and compare roughness factors of prepared materials. From noticing 2D and 3D images of compounds $\text{SiO}_2@\text{Ni(II)}$ and $\text{SiO}_2@\text{Ni(0)}$ in Figure. 3.6, it is clear that the topography of the prepared samples is very clear. Table 3.2 shows the roughness factors of both samples. The roughness parameters, show that the factor in $\text{SiO}_2@\text{Ni(0)}$ is higher than $\text{SiO}_2@\text{Ni(II)}$. This can be attributed to the formation of nickel nanoparticles on the surface of the silica in the form of atoms, which are by nature larger in size than the ions from which they were formed.

Table 3-2 Roughness parameters of SiO₂@Ni(II) and SiO₂@Ni(0)

Compound	Average roughness(Ra)	Square root roughness (Rrms)	Height of ten points(Sz)
SiO ₂ @Ni(II)	235 pm	301 pm	2.98 nm
SiO ₂ @Ni(0)	492.50 pm	641 pm	5.17 nm

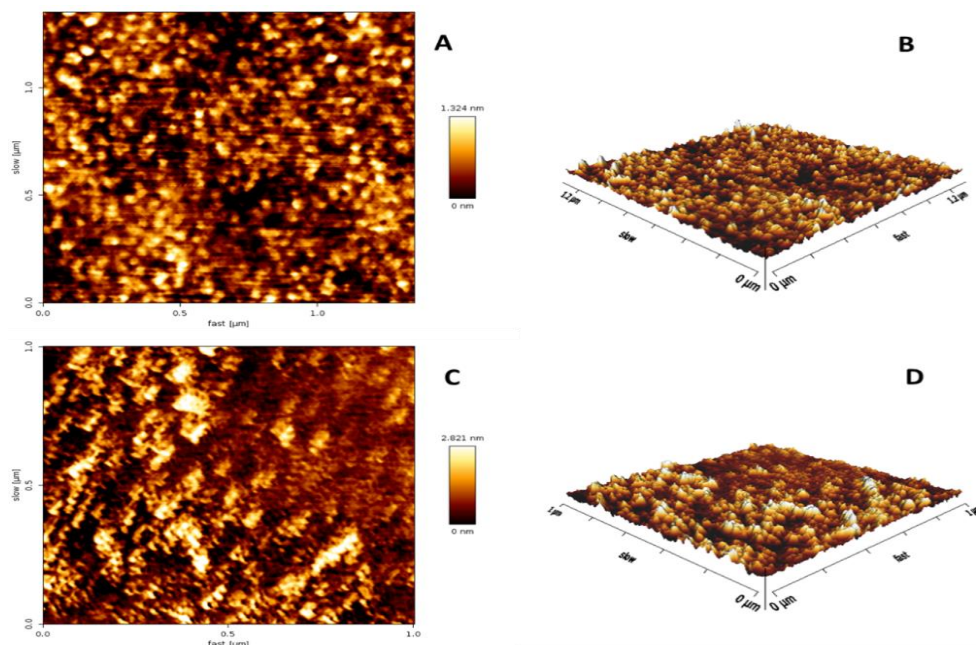


Figure. 3.6 A & B Two-dimensional and three-dimensional images of SiO₂@Ni(II), C & D Two-dimensional and three-dimensional images of SiO₂@Ni(0).

3.1.7 Thermogravimetric Analysis (TGA-DSC)

The thermal characteristics of nickel-silica nanoparticles SiO₂@Ni(II) and SiO₂@Ni(0) were investigated using Thermal Gravimetric Analysis (TGA-DSC) techniques. Figure. 3.7A shows the TGA-DSC of the SiO₂@Ni(II) material. It was noted that the total loss percentage was 27.41% in the temperature range of 30-900°C. The weight loss of silica below 270 °C is ≈ 8% at an exothermic peak of 101°C from the DSC curve, which is attributed to the decomposition of physically absorbed water with silica [102, 112] and the mass loss (18%) from

270 to 600 °C is related to the transformation of silanol Si-OH groups into Si-O-Si siloxanes in the structure of SiO₂@Ni(II) [55]. The remainder of the temperature curve at 600-900 °C can be attributed to the formation of NiO. Figure.3.7(B) shows the thermogravimetric decomposition (DTD-DSC) of the SiO₂@Ni(0) sample, as it was noted that the total loss percentage of 12.50% in the temperature range 30-900°C. Which is much less than the thermal decomposition of the SiO₂@Ni(II), so this can be attributed to the fact that most of the Ni(II) ions (NiO) in the SiO₂@Ni(II) material are converted into nickel nanoparticles in the free atoms due to the use reducing agent NaBH₄. The first loss of 6% within the temperature range of 30-300°C signifies the evaporation of water that was previously adsorbed, which was physically trapped by SiO₂@Ni(0). The second decomposition percentage of 6.50% occurs in the range of 300-600 °C. It can refer to the transformation of silanol Si-OH groups into Si-O-Si siloxanes in the structure of SiO₂@Ni(0).

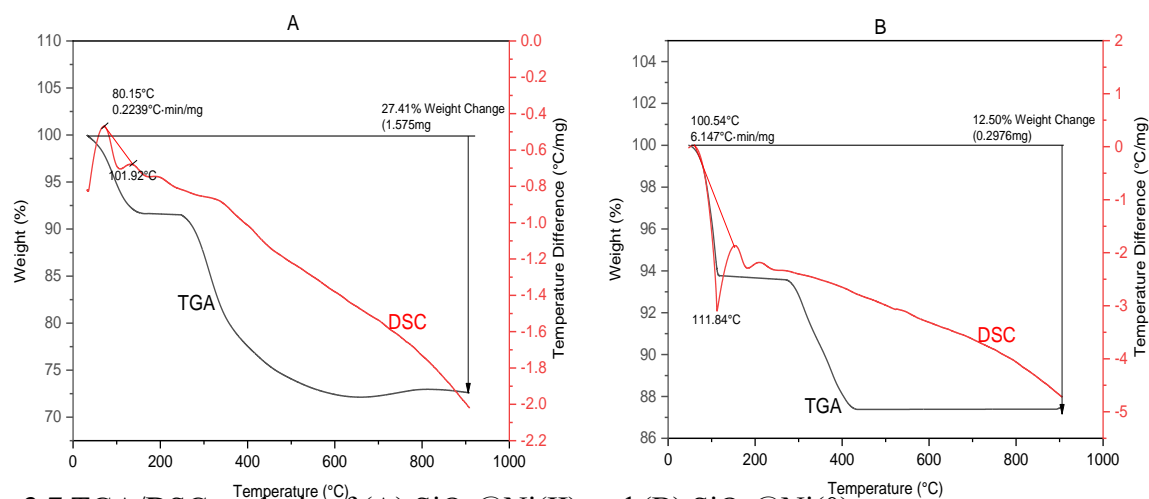


Fig. 3.7 TGA/DSC analysis of (A) SiO₂@Ni(II) and (B) SiO₂@Ni(0)

3.1.8 UV–Vis (DRUV–Vis) Absorption Spectra

One of the important physical measurements, in which the geometric environment of the transition metal ion in solid materials is studied, is diffuse

reflectance visible (DR-UV/VIS) spectroscopy. Figure.3.8 shows the diffuse reflectance of UV–vis (DRUV–vis) absorption spectra of the $\text{SiO}_2@\text{Ni(II)}$ and $\text{SiO}_2@\text{Ni(0)}$. The spectrum of the compound $\text{SiO}_2@\text{Ni(II)}$ showed many absorption bands in the regions 300, 400, 680, and 740 nm. The first peak at 300 can be attributed to charge transfer bands with the nickel(II) ion and the oxygen ion in the mesoporous silica framework[110], related to an $\text{O}^{2-} (2p) \rightarrow \text{Ni}^{2+} (3d)$ charge transfer transition in the mesoporous lattice[115]. This transition can be attributed to the transfer to the NiO formed within the silica lattice or to the electronic transfer between the oxygen ion bound to the silica (Si-O^{2-}) and Ni^{2+} [110, 116]. The $\text{SiO}_2@(\text{Ni(II)})$ also shows absorption bands at 400, 680, and 740 nm attributed to electron transitions ${}^3\text{A}_{2g}(\text{F}) \rightarrow {}^3\text{T}_{1g}(\text{P})$, ${}^3\text{A}_{2g}(\text{F}) \rightarrow {}^3\text{T}_{2g}(\text{F})$ and ${}^3\text{A}_{2g}(\text{F}) \rightarrow {}^3\text{T}_{1g}(\text{F})$ in octahedral coordination in NiO. Fig. 7 also showed the diffuse reflectance spectrum of compound $\text{SiO}_2@(\text{Ni(0)})$ after adding the reducing agent NaBH_4 to $\text{SiO}_2@(\text{Ni(II)})$. It was observed that the intensity of the electronic d-d transitions decreased significantly, especially the transition in the region of 400 nm. The appearance of a strong band of intensity at 300 nm can be explained by the reduction. It was not done completely, as the Ni(II) ions are embedded in the silica matrix, and thus, a portion of them remains in the form of free ions. To determine the nickel content in the prepared materials $\text{SiO}_2@(\text{Ni(II)})$ and $\text{SiO}_2@(\text{Ni(0)})$, inductively coupled plasma mass spectrometry (ICP-MS) was used. The results showed that the nickel-modified silica particles $\text{SiO}_2@(\text{Ni(II)})$ and $\text{SiO}_2@(\text{Ni})$ containing 78 and 100 mg/mL of nickel, respectively, confirming the previously discussed results indicating the presence of nickel in the silicon network of the prepared materials.

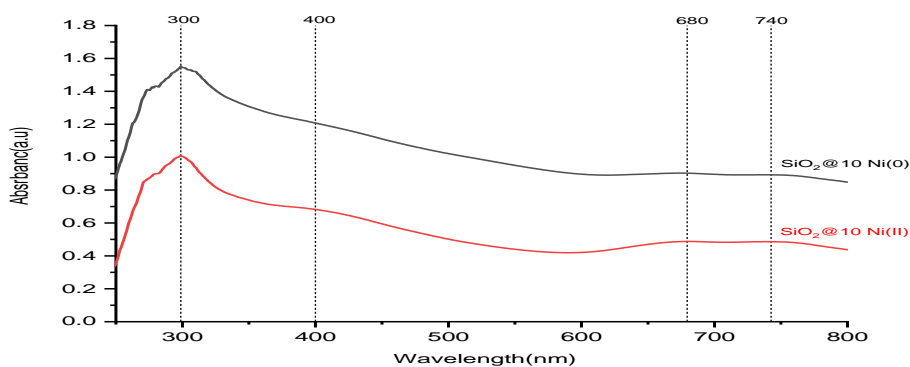


Figure. 3.8. DRUV–vis spectra of SiO₂@Ni(II) and (B) SiO₂@Ni(0) composites

3.1.9 X-Ray Photoelectron Spectroscopy (XPS)

The elemental compositions on the surface of the nickel-silica nanoparticles SiO₂@Ni(II) and (B) SiO₂@Ni(0) were identified by XPS spectroscopy. This technique also gives us information about the oxidation state of nickel in the prepared samples. Figure.3.9 shows the XPS spectra of the sample elements separately of the nickel-silica nanoparticles SiO₂@Ni(II) and SiO₂@Ni(0). The XPS spectrum of the oxygen (O, 1s) level (Fig.3.9 A) in the SiO₂@Ni(II) and SiO₂@Ni(0) have been showed a sharp peak at 531.8 eV and 532.45 eV respectively, clearly indicating the presence of oxygen ions within the SiO₂ [19, 117]. The binding energy of silicon (Si, 2p) in the SiO₂@Ni(II) and SiO₂@Ni(0) nanoparticles (Fig.3.9 B) was 103.71 and 103.16 eV, respectively, indicating that silicon exists mainly in the form of SiO_n. The oxidation states of nickel incorporated on the surface of SiO₂@Ni(II) and SiO₂@Ni(0) nanoparticles were studied by X-ray photon electron spectroscopy (XPS). the XPS spectrum of the nickel (Ni, 2p) level in SiO₂@Ni(II) and SiO₂@Ni(0) exhibits two characteristic double peaks split by spin–orbit coupling of 2p_{1/2} and 2p_{3/2} in the range (≈870–885 eV) and (≈852–865 eV), respectively[118]. The observed photon peaks at 852.8 and 872.9 eV can be attributed to metallic Ni⁰, while the observed photon peaks at 855.8 and 879.8 eV can be attributed to Ni²⁺ [119]. which is in good

agreement with previous reports on metallic nickel and nickel oxide compounds [119]. These results indicate the in situ formation of metallic nickel during the reaction between nickel acetate tetrahydrate and sodium silicate derived from rice husk. And also indicates that the oxidation states of nickel in the nickel-silica nanoparticles range between Ni^0 and Ni^{2+} , which is consistent with the XPS results (Fig. 3.9 C).

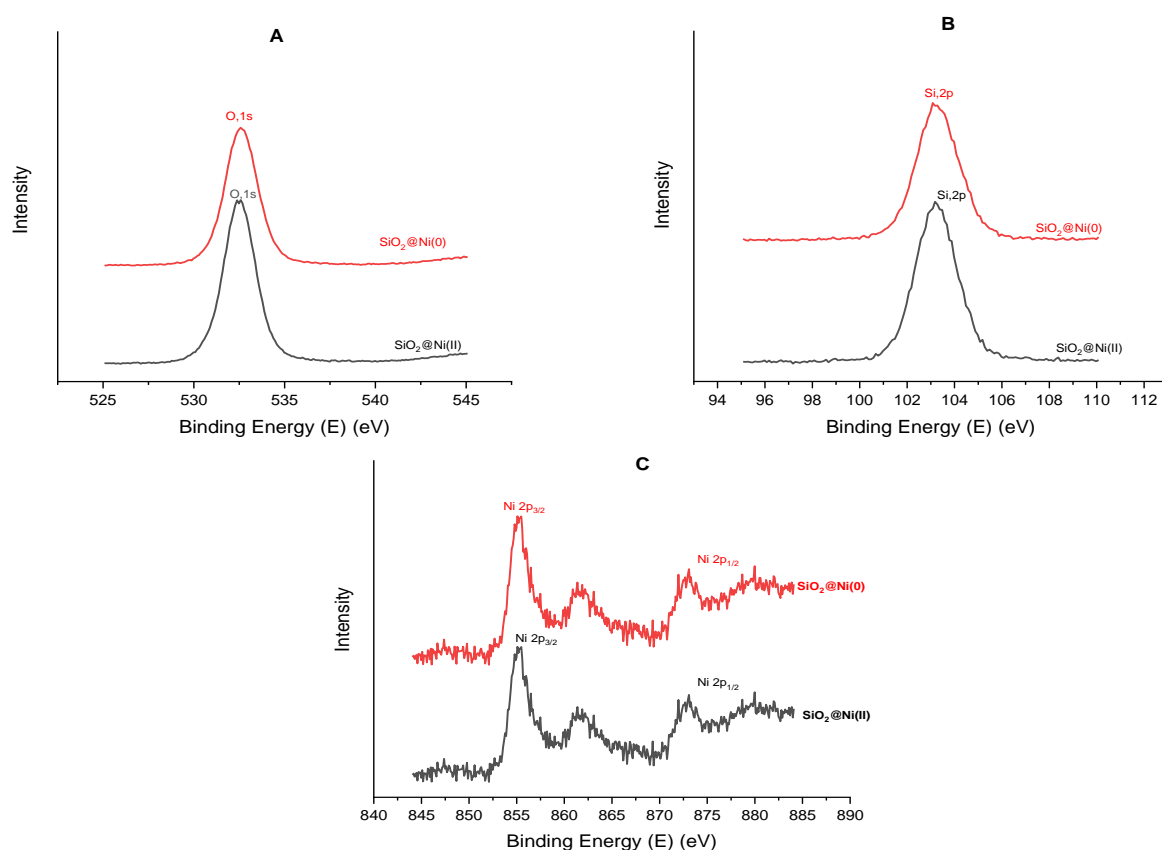


Figure. 3.9 The O 1s (A), Si 2p (B) and Ni 2p (C) X-ray photoelectron spectra of nickel-silica nanoparticles SiO₂@Ni(II) and (B) SiO₂@Ni(0)

3.1.10 Evaluation of Antibacterial Activity

The antibacterial activity Figure.3.10 of nickel-silica nanoparticles SiO₂@Ni(II) and SiO₂@Ni(0) against *E. coli* and *S. aureus* compared with DMSO as a negative control. Table 3.3 shows that the inhibitory effect of the studied compounds increases with increasing concentration. Also, Table 3.3 shows the

disappearance of any bacterial growth at high concentrations of $\text{SiO}_2@\text{Ni(II)}$ and $\text{SiO}_2@\text{Ni(0)}$ compared to the studied compounds with lower concentrations. Through the diameters of inhibition in Table 3.3, it appears that the inhibition of *S. aureus* bacteria is somewhat greater than that of *E. coli* bacteria. This is consistent with some previous studies [120, 121]. The present study showed that silica nanoparticles $\text{SiO}_2@\text{Ni(II)}$ and $\text{SiO}_2@\text{Ni(0)}$ gave high inhibition compared to the antibiotic ciprofloxacin. Table 3.4 shows the minimum inhibitory concentration for $\text{SiO}_2@\text{Ni(II)}$ and $\text{SiO}_2@\text{Ni(0)}$. From the values mentioned in Table 3.4, it is clear that the MIC is 3.125 and 12.50 mg/mL of $\text{SiO}_2@\text{Ni(II)}$ and $\text{SiO}_2@\text{Ni(0)}$, respectively, which killed all bacterial cells in *E.coli*. Meanwhile, the concentrations of 3.125 and 6.25 mg/mL of $\text{SiO}_2@\text{Ni(II)}$ and $\text{SiO}_2@\text{Ni(0)}$, respectively, are the MIC that killed all bacterial cells in *S .aureus*. The antibacterial activity of silica-nickel nanoparticles can be attributed to several reasons: Gram-negative bacteria *E.coli* have thin inner membranes with a triangular cell wall and an outer membrane (OM). In contrast, the Gram-positive bacteria *S. aureus* has no OM layers. Thus, *E. coli* is more resistant to chemical compounds [122]. The generation of reactive oxygen species (ROS) that destroy DNA and protein. Many references indicate that the generation of ROS resulting from oxidative stress is the main factor for the antibacterial activity of silica compounds. Thus, this factor leads to severe damage to cells, including DNA and protein, leading to cell death [123, 124]. Another reason that leads to inhibition of bacterial growth is the size, shape, and surface charge of silica compounds, which leads to cell death. In addition to that, the positive charge of the metal ions affects negatively charged bacteria, especially *E. coli*. Thus, this interference leads to the inactivation of cellular enzymes and then the permeability of the membrane [125].

Table 3-3 The antibacterial effect of SiO₂@Ni(II) and SiO₂@Ni(0) against *E. coli* and *S. aureus*

Nickel-silica nanoparticles	Con. mg/mL	Inhibition zone(mm) of <i>E. coli</i> by SiO ₂ @Ni(II)	Inhibition zone(mm) of <i>E. coli</i> by SiO ₂ @Ni(0)
	100	23 ± 1.5	22.5 ± 1.2
	80	18 ± 1.0	16 ± 0.8
	60	16.5 ± 0.6	14 ± 0.5
	40	11.5 ± 0.4	9 ± 0.3
	20	5 ± 0.2	4 ± 0.1
	Inhibition average	14.8 ± 0.74	13.1 ± 0.58
	L.S.D at 0.05	2.5	2.19
	DMSO	nill	nill
	Control positive (Ciprofloxacin)mm in diameter Antibiotic 5mg/disc	9	
Nickel-silica nanoparticles	Con. mg/mL	Inhibition zone(mm) of <i>S. aureus</i> by SiO ₂ @Ni(II)	Inhibition zone(mm) of <i>S. aureus</i> by SiO ₂ @Ni(0)
	100	26 ± 1.5	24± 1.7
	80	20± 1.2	18± 1.03
	60	14± 0.8	13.5± 0.94
	40	13.5± 0.53	10± 0.88
	20	6.5± 0.32	4.5± 0.34
	Inhibition average	16± 0.87	14± 0.978
	L.S.D at 0.05	2.35	2.04
	Control positive (Ciprofloxacin) mm in diameter Antibiotic 5mg/disc	6	

Table 3-4 Minimum inhibitory concentration (MIC) mg/mL for SiO₂@Ni(II) and SiO₂@Ni(0) against *E. coli* and *S. aureus*.

Minimum inhibitory concentration(MIC) mg/mL against <i>E. coli</i>						
Nickel-silica nanoparticles	Concentration (mg/mL)					
	50	25	12.50	6.25	3.125	1.5625
SiO ₂ @Ni(II)	-	-	-	-	-	+
SiO ₂ @Ni(0)	-	-	-	+	+	+

Minimum inhibitory concentration(MIC) mg/mL against <i>S. aureus</i>						
Nickel-silica nanoparticles	Concentration (mg/mL)					
	50	25	12.50	6.25	3.125	1.5625
SiO ₂ @Ni(II)	-	-	-	-	-	+
SiO ₂ @Ni(0)	-	-	-	-	+	+

- no growth + growth

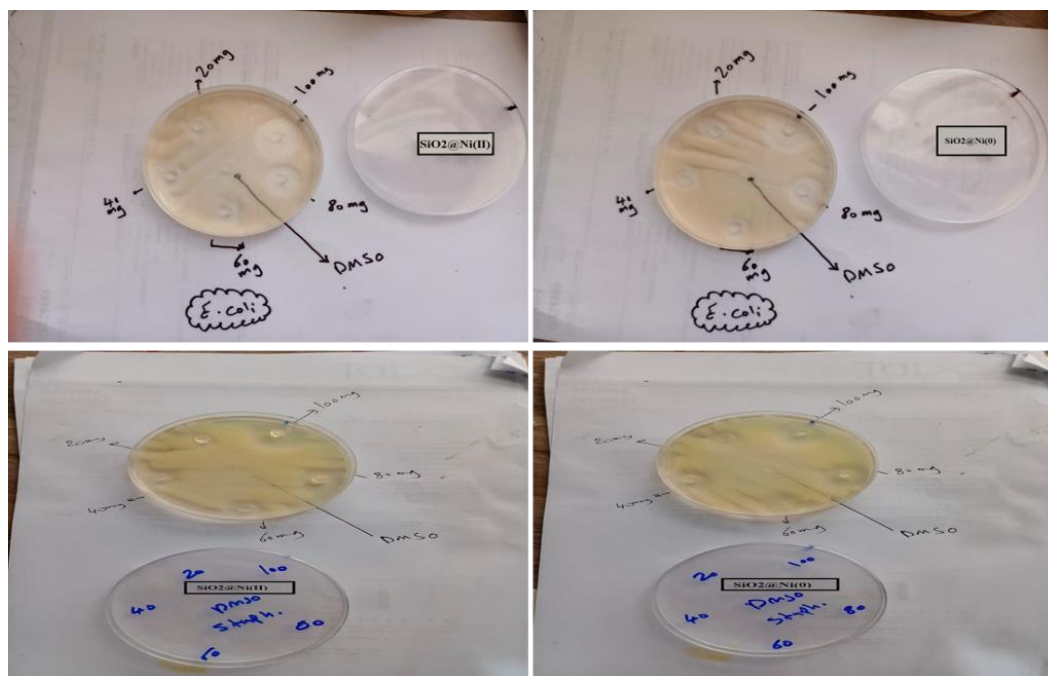
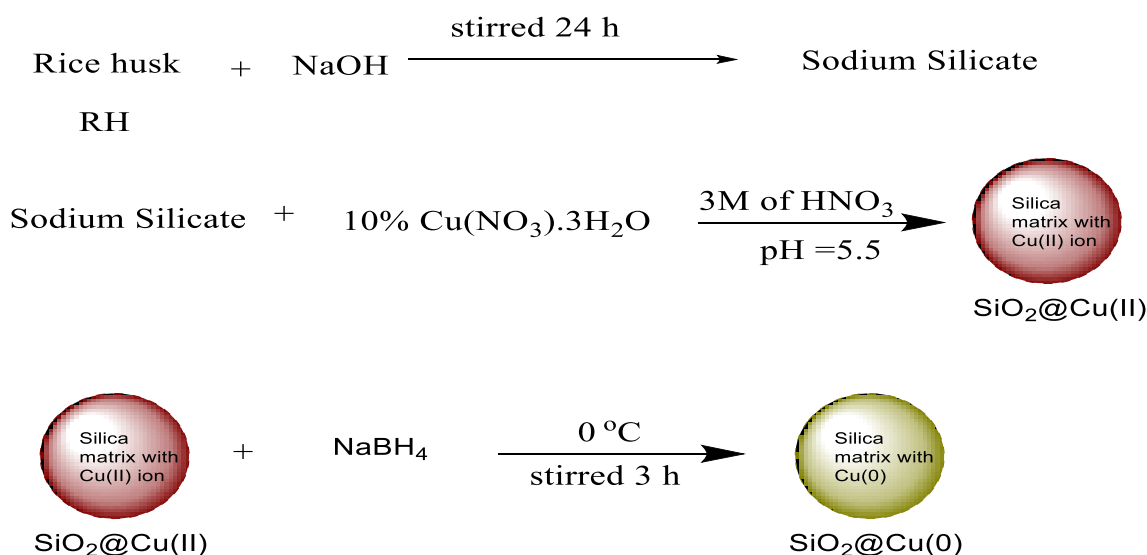


Figure.3.10 Antibacterial activity of nickel-silica nanoparticles SiO₂@Ni(II) and SiO₂@Ni(0) against *E.coli* and *S.aureus* in different concentrations 20, 40, 60, 80 and 100 mg/mL.

3.2 Synthesis and Characterization of SiO₂@Cu(II) and SiO₂@Cu(0)

To the solution of sodium silicate, 3 M HNO₃ containing 10 wt.% of Cu(NO₃)₂.3H₂O was added. The appearance of the gel began at pH 10 until reached 5.5. A sufficient. The resulting solution containing the dark nutty gel was set aside for 24 hr. After aging. The gel separated by centrifugation using a Hettich centrifuge at a speed of 4000 revolutions per minute. After that dried in an oven at a temperature of 110 °C and labeled as SiO₂@Cu(II). About 1.0 g of SiO₂@Cu(II) was dissolved in 50 mL of cold deionized water, Then, an excess of NaBH₄ as a reducing agent (2.0 g) was added and then stirred vigorously in an ice bath for three hours. During this time, the color of the suspension was changed from dark nutty to light olive. After that, a colored precipitate was obtained, filtered, washed with deionized water several times, and placed in the oven at 110 °C for a whole day. After cooling it, 0.9 g of the final product was obtained, labeled as SiO₂@Cu(0), A schematic diagram of the method for preparing SiO₂@Cu(II) and SiO₂@Cu(0) is shown in Scheme 3.2.



Scheme 3.2 Preparation of SiO₂@Cu(II) and SiO₂@Cu(0) from rice husk

3.2.1 Fourier Transform Infrared Spectroscopy (FTIR)

The synthesized copper-silica nanoparticles $\text{SiO}_2@\text{Cu(II)}$ and $\text{SiO}_2@\text{Cu(0)}$ were characterized using FTIR spectroscopy (Figure.3.11). The spectra of $\text{SiO}_2@\text{Cu(II)}$ and $\text{SiO}_2@\text{Cu(0)}$ showed the typical absorption bands around 3430 cm^{-1} , which are assigned to stretching vibrations of silanol (Si-OH) and stretching vibrations of physically absorbed water with silica [55, 100, 101]. The absorption bands around 1635 cm^{-1} are ascribed to the bending vibrations of absorbed water with silica surface[6, 102]. The absorption bands around 800 cm^{-1} and 1180 cm^{-1} are ascribed to the symmetric and antisymmetric stretching vibrations of siloxane group (Si-O-Si), respectively [103, 104]. The stretching vibrations of Cu-O-Si appeared around 830 cm^{-1} [105, 106], and it was noted that it disappeared in $\text{SiO}_2@\text{Cu(0)}$ due to the reduction of Cu(II) to Cu(0) . The actual locations of all peaks are shown in Figure.3.11.

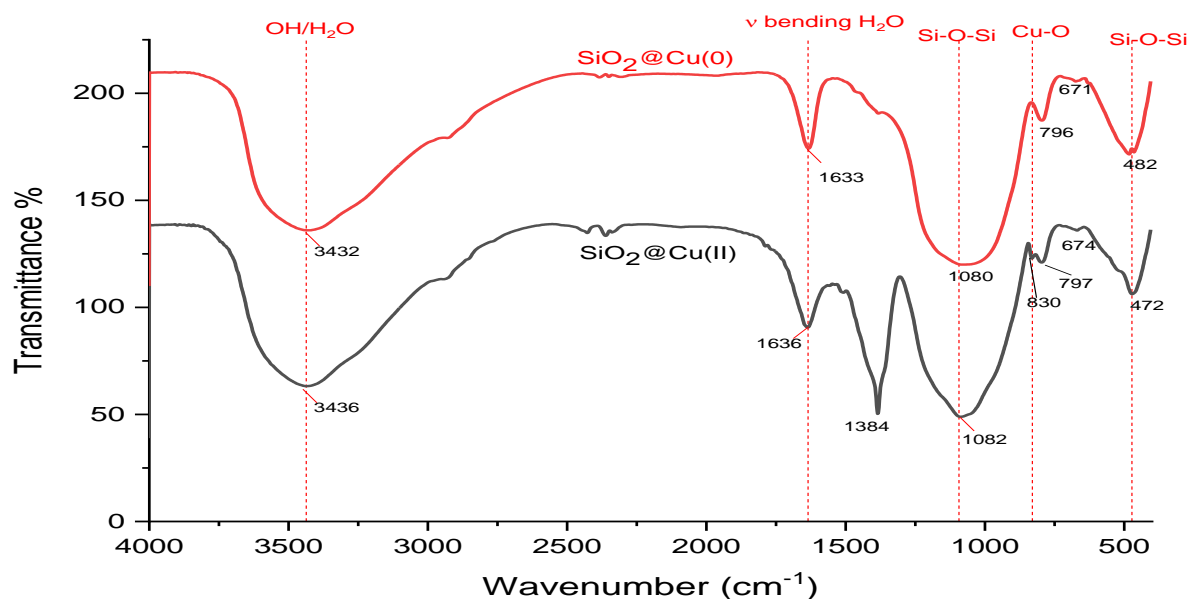


Figure. 3.11 FTIR spectra of $\text{SiO}_2@\text{Cu(II)}$ and $\text{SiO}_2@\text{Cu(0)}$

3.2.2 X-Ray Diffraction Analysis (XRD)

XRD patterns of copper-silica nanoparticles particles $\text{SiO}_2@\text{Cu}(\text{II})$ and $\text{SiO}_2@\text{Cu}(0)$ were offered in Figure. 3.12. In both patterns, a broad peak around 26 of 2θ is observed, which is characteristic of amorphous silica [32, 107]. The sharp peaks characteristic of copper oxide are not observed in $\text{SiO}_2@\text{Cu}(\text{II})$ and $\text{SiO}_2@\text{Cu}(0)$, but instead broad peaks of copper metal are observed at $2\theta = 36^\circ$ in both $\text{SiO}_2@\text{Cu}(\text{II})$ and $\text{SiO}_2@\text{Cu}(0)$, and at $2\theta = 46^\circ$ and 63° for $\text{SiO}_2@\text{Cu}(\text{II})$ which reveal the weak crystal structure of $\text{SiO}_2@\text{Cu}(\text{II})$ and $\text{SiO}_2@\text{Cu}(0)$. These results are consistent with other references [108–110].

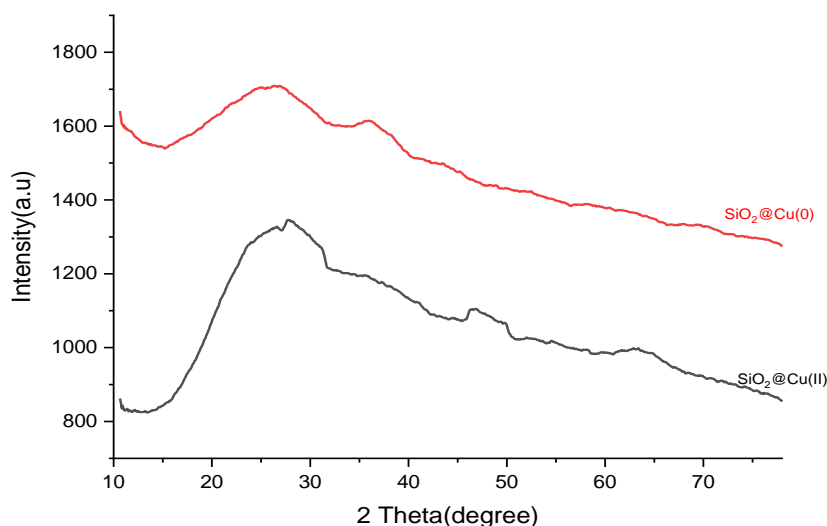


Figure.3.12 The XRD pattern of $\text{SiO}_2@\text{Cu}(\text{II})$ and $\text{SiO}_2@\text{Cu}(0)$

3.2.3 N_2 Adsorption/Desorption Analysis

The porosity, surface area and capillary structure of copper-silica particles $\text{SiO}_2@\text{Cu}(\text{II})$ and $\text{SiO}_2@\text{Cu}(0)$ were studied by N_2 - adsorption/desorption technique as shown in Figures. 3.13 A&B, separately. The isotherms and their hysteresis loops were from type IV and H3, respectively[98, 107, 111, 113]. This

preres that the prepared materials are mesoporous materials, where interactions between gas molecules and the absorbent mesoporous surface lead to capillary condensation. The inset in Figure.3.13 shows the corresponding pore size distribution for both materials $\text{SiO}_2@\text{Cu(II)}$ and $\text{SiO}_2@\text{Cu(0)}$, as the pore distribution falls within the range of 2-10 nm, which fall in the mesoporous range. Table 3.5 shows the result of N_2 -adsorption/desorption analysis of $\text{SiO}_2@\text{Cu(II)}$ and $\text{SiO}_2@\text{Cu(0)}$. The specific surface area, average pore volume and mean pore diameter of $\text{SiO}_2@\text{Cu(0)}$ larger compared of $\text{SiO}_2@\text{Cu(II)}$ due to the size of copper in form as metal. This may be due to the fact that silica-Cu(0) nanoparticles are larger in size than silica-Cu(II) nanoparticles.

Table3-5 The result of N_2 - adsorption/desorption analysis of $\text{SiO}_2@\text{Cu(II)}$ and $\text{SiO}_2@\text{Cu(0)}$

Compound	Specific surface area(m^2/g)	Average pore volume ($\text{cm}^3 \text{g}^{-1}$)	Mean pore diameter (nm)
$\text{SiO}_2@\text{Cu(II)}$	80.143	0.188	9.423
$\text{SiO}_2@\text{Cu(0)}$	100.980	0.341	13.510

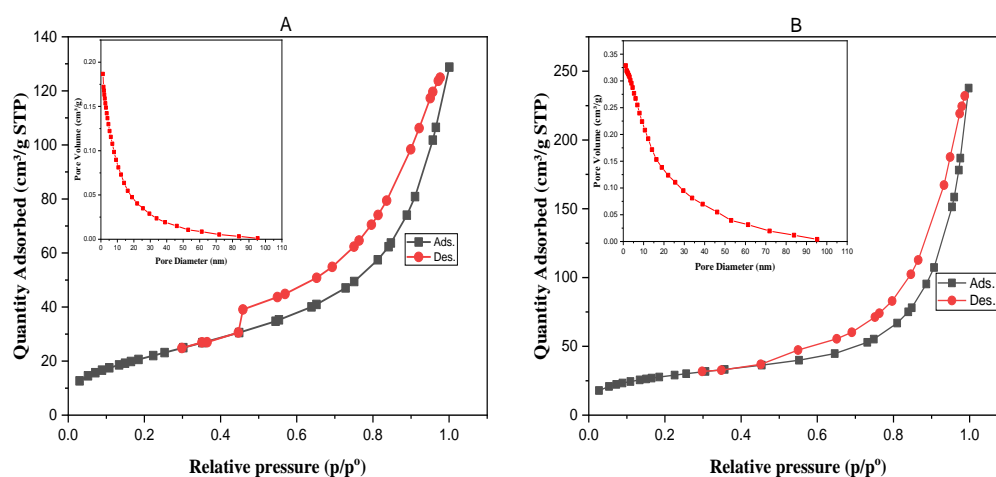


Figure. 3.13 The N_2 adsorption/desorption isotherms of (A) $\text{SiO}_2@\text{Cu(II)}$ and (B) $\text{SiO}_2@\text{Cu(0)}$. The inset shows the corresponding pore size distribution.

3.2.4 Field Emission Scanning Electron Microscopy (FESEM) Analysis

The morphology of the prepared nanoparticles $\text{SiO}_2@\text{Cu(II)}$ and $\text{SiO}_2@\text{Cu(0)}$ (Figure.3.14 A&C) were observed by FESEM. All the nanoparticles of $\text{SiO}_2@\text{Cu(II)}$ and $\text{SiO}_2@\text{Cu(0)}$ showed a homogeneous spherical structure and uniformly dispersed. In addition, the average particle size was in the range of 50-150 nm which was consistent with mesoporous and macroporous range [77, 114]. The spectra of EDX for $\text{SiO}_2@\text{Cu(II)}$ and $\text{SiO}_2@\text{Cu(0)}$ were showed in Figure.3.14 B&D. The basic elements (silicon and oxygen) in the samples were observed, in addition to the presence of copper element. This can be considered supportive evidence for the success of the process of preparing copper-supported silica particles.

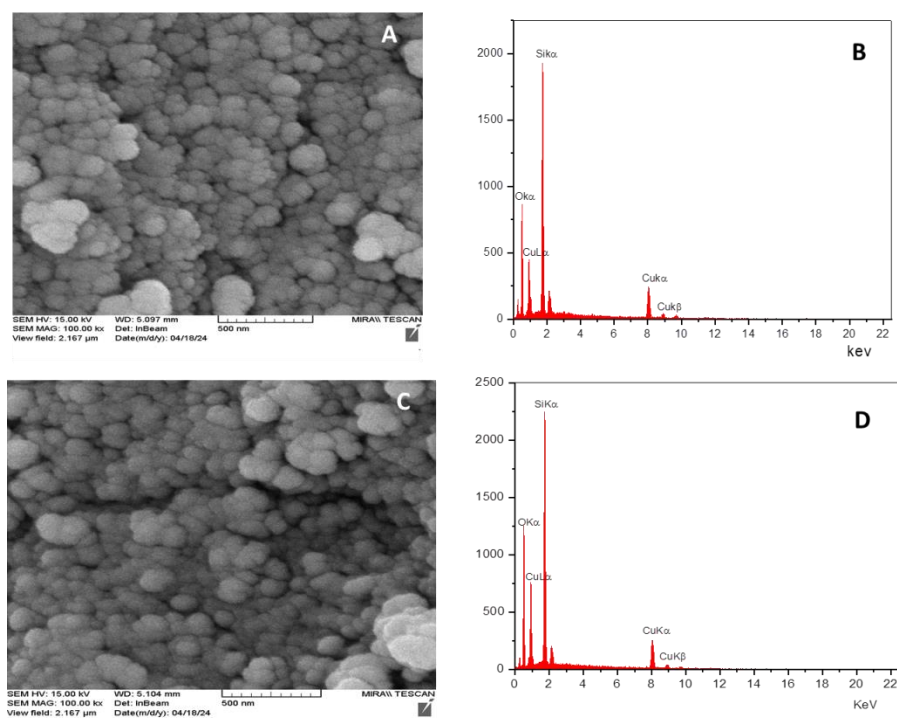


Figure.3.14 A & B FESEM-EDX for $\text{SiO}_2@\text{Cu(II)}$, C & D FESEM-EDX for $\text{SiO}_2@\text{Cu(0)}$

3.2.5 Transmission Electron Microscopy (TEM) Analysis

The transmission electron microscope images Figure.3.15 clearly indicate the core-shell structure of $\text{SiO}_2@\text{Cu(II)}$ and $\text{SiO}_2@\text{Cu(0)}$, revealing that the silica

particles were successfully incorporated with the copper nanoparticles. Also, the $\text{SiO}_2@\text{Cu(II)}$ image showed homogeneously distributed granular spots with a diameter ranging between 5-7nm that could be attributed to copper oxides. The image of $\text{SiO}_2@\text{Cu(0)}$ showed dark black spots that could be attributed to copper nanoparticles with a diameter ranging between 9-20nm. This is greater than that of the unreduced silica-copper particles $\text{SiO}_2@\text{Cu(II)}$ and this is consistent with the result of N_2 - adsorption/desorption measurements.

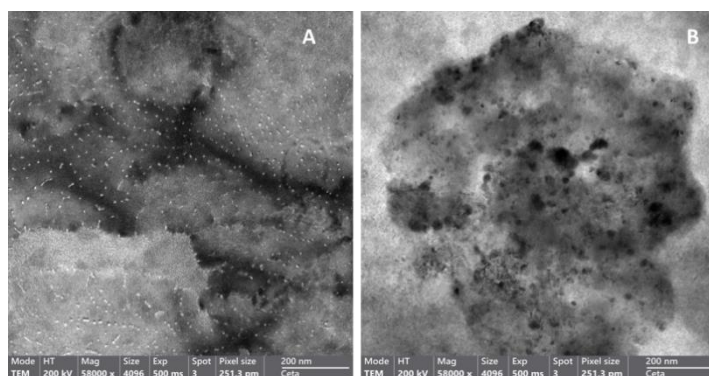


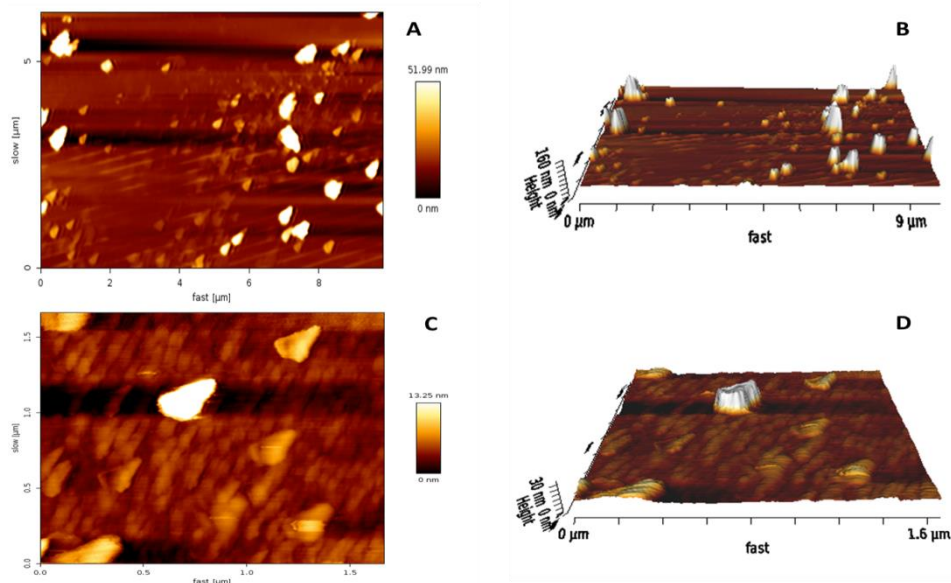
Figure.3.15 A The TEM images of A- $\text{SiO}_2@\text{Cu(II)}$ and B- $\text{SiO}_2@\text{Cu(0)}$

3.2.6 Atomic Force Microscopy (AFM)

The high-resolution two-dimensional and three-dimensional images of $\text{SiO}_2@\text{Cu(II)}$ and $\text{SiO}_2@\text{Cu(0)}$ were showed in Figure.3.16. Furtherly the roughness factors of prepared materials were showed in Table 3.6. From observing the 2D and 3D images of compounds $\text{SiO}_2@\text{Cu(II)}$ and $\text{SiO}_2@\text{Cu(0)}$, it is clear that the topography of the prepared samples are very clear. The roughness parameters (average roughness(Ra), square root roughness (Rrms) and height of ten points(Sz)) of $\text{SiO}_2@\text{Cu(II)}$ are higher than $\text{SiO}_2@\text{Cu(0)}$, and this can be attributed to the formation of copper nanoparticles on the surface of the silica in the form of ions, which are by nature larger in size than the atoms from which they were formed.

Table 3-6 Roughness parameters of SiO₂@Cu(II) and SiO₂@Cu(0)

Compound	Average roughness(Ra)	Square root roughness (Rrms)	Height of ten points(Sz)
SiO ₂ @Cu(II)	4.941 nm	11.82 nm	161.8 nm
SiO ₂ @Cu(0)	1.484 nm	3.010 nm	33.51 nm

**Figure.3.16** A & B Two-dimensional and three-dimensional images of SiO₂@Cu(II), C & D Two-dimensional and three-dimensional images of SiO₂@Cu(0).

3.2.7 Thermogravimetric Analysis (TGA-DSC)

Thermal gravimetric analysis (TGA-DSC) measurements were performed to study the thermal properties of copper-silica nanoparticles SiO₂@Cu(II) and SiO₂@Cu(0). Figure. 3.17A shows the TGA-DSC of the SiO₂@Cu(II) material. It was noted that the total loss percentage of 28.94% in the temperature range 30-900°C. The weight loss of silica below 240 °C is ≈ 6% at an endothermic peak of 77.02°C from the DSC curve which is attributed to the decomposition of physically absorbed water with silica [102, 112] , and the mass loss about (23%) from 240 to 900 °C is related to the transformation of silanol Si-OH groups into

Si-O-Si siloxanes in the structure of $\text{SiO}_2@\text{Cu(II)}$ and formation of CuO [55]. Figure.3.17(B) shows the thermogravimetric decomposition (DTG-DSC) of the $\text{SiO}_2@\text{Cu(0)}$ sample, as it was noted that the total loss percentage of 4.81% in the temperature range 30-900°C which is much less than the thermal decomposition of the $\text{SiO}_2@\text{Cu(II)}$. This can be attributed to the fact that most of the Cu(II) ions (CuO) in the $\text{SiO}_2@\text{Cu(II)}$ material are converted into copper nanoparticles in the free atoms due to the use reducing agent NaBH_4 . The first loss percentage of 2.50% in the temperature range 30-300°C indicates the loss of evaporation of adsorbed water which was trapped physically $\text{SiO}_2@\text{Cu(0)}$. The second decomposition percentage of 1.50% occurs in the range of 300-600 °C can be refers transformation of silanol Si-OH groups into Si-O-Si siloxanes in the structure of $\text{SiO}_2@\text{Cu(0)}$ and formation of copper nanoparticles in metal formula.

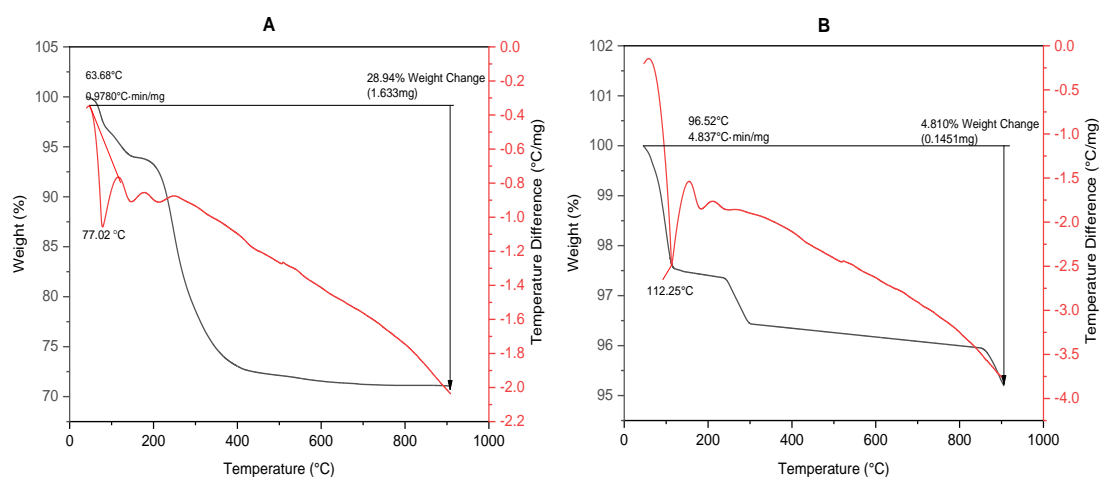


Figure.3.17 TGA/DSC analysis of (A) $\text{SiO}_2@\text{Cu(II)}$ and (B) $\text{SiO}_2@\text{Cu(0)}$

3.2.8 UV–Vis (DRUV–Vis) Absorption Spectra

The $\text{SiO}_2@\text{Cu(II)}$ and (B) $\text{SiO}_2@\text{Cu(0)}$ nanoparticles were characterised by diffuse reflectance UV-vis spectroscopy (DRUV-vis). The DRUV-vis of $\text{SiO}_2@\text{Cu(II)}$ and (B) $\text{SiO}_2@\text{Cu(0)}$ are shown in Figure.3.18. The spectrum of the

compound $\text{SiO}_2@\text{Cu(II)}$ showed many absorption bands in the regions 306, 350, 430, 700, and 760 nm. The first three peaks at 306, 350 and 430 can be attributed to charge transfer bands with the copper(II) ion and the oxygen ion in the mesoporous silica framework, related to a $\text{O}^{2-}(2p) \rightarrow \text{Cu}^{2+}(3d)$ charge transfer transition in the mesoporous lattice [126]. This transition can be attributed to the transfer to the CuO formed within the silica lattice. On the other hand, the $\text{SiO}_2@\text{Cu(II)}$ also shows a broad absorption band in the range 600-800 nm attributed to electron transitions ${}^2\text{E}_g \rightarrow {}^2\text{T}_{2g}$ in octahedral coordination in CuO [127, 128]. Fig. 3.18 also showed the diffuse reflectance spectrum of compound $\text{SiO}_2@(\text{Cu(0)})$ after adding the reducing agent NaBH_4 to $\text{SiO}_2@(\text{Cu(II)})$. It was observed that the intensity of the electronic d-d transitions decreased significantly, especially the transition in the region of the range 300-450 nm. The appearance of a strong band of intensity at 306 nm can be explained by the reduction that was not done completely, as the Cu(II) ions are embedded in the silica matrix, and thus a portion of them remains in the form of free ions.

To determine the copper content in the prepared materials $\text{SiO}_2@(\text{Cu(II)})$ and $\text{SiO}_2@(\text{Cu(0)})$, inductively coupled plasma mass spectrometry (ICP-MS) was used. The results showed that the copper-silica nanoparticles particles $\text{SiO}_2@(\text{Cu(II)})$ and $\text{SiO}_2@(\text{Cu(0)})$ containing 100 mg/mL of copper, confirming the previously discussed results indicating the presence of copper in the silicon network of the prepared materials.

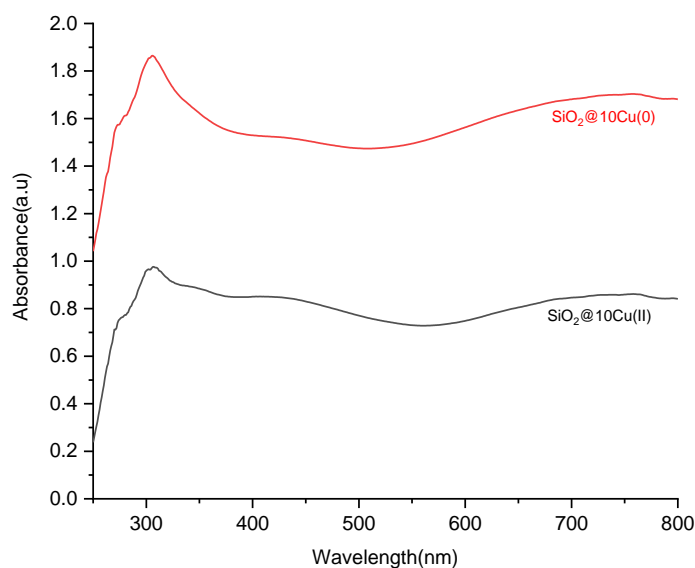


Figure. 3.18. DRUV–vis spectra of $\text{SiO}_2\text{@Cu(II)}$ and (B) $\text{SiO}_2\text{@Cu(0)}$ composites

3.2.9 Evaluation of Antibacterial Activity

The antibacterial activity (Figure.3.19) of copper-silica nanoparticles $\text{SiO}_2\text{@Cu(II)}$ and $\text{SiO}_2\text{@Cu(0)}$ against *E. coli* and *S. aureus* compared with DMSO as a negative control was studied. Table 3.7 shows that the inhibitory effect of the studied compounds increases with increasing concentration. Also, Table 3.7 shows the disappearance of any bacterial growth at high concentrations of $\text{SiO}_2\text{@Cu(II)}$ and $\text{SiO}_2\text{@Cu(0)}$ compared to the studied compounds with lower concentrations. Through the diameters of inhibition in Table 3.7, it appears that the inhibition on *S. aureus* bacteria is somewhat higher than *E. coli* bacteria. This is consistent with some previous studies.

Table 3.8 showed the minimum inhibitory concentration (MIC) for $\text{SiO}_2\text{@Cu(II)}$ and $\text{SiO}_2\text{@Cu(0)}$. From the values mentioned in Table 3.8, it is clear that the MIC is 6.25 and 3.125 mg/mL of $\text{SiO}_2\text{@Cu(II)}$ and $\text{SiO}_2\text{@Cu(0)}$, respectively, which killed all bacterial cells in *E. coli*. In contrast the concentration of 3.125 mg/mL of $\text{SiO}_2\text{@Cu(II)}$ and $\text{SiO}_2\text{@Cu(0)}$ is the MIC that killed all bacterial cells in *S.*

aureus. The antibacterial activity of silica-copper nanoparticles can be attributed to several reasons: One of the main factors that lead to killing bacteria and thus destroying DNA and protein is the formation of reactive oxygen species (ROS), as many studies indicate that the formation of (ROS) resulting from oxidative stress is the main factor for the antibacterial activity of silica nanoparticles. Thus, this factor leads to severe damage to cells, leading to their death[123, 124].

Another reason that leads to inhibition of bacterial growth is the size, shape, and surface charge of silica nanoparticles, which leads to cell death [129]. Additionally, the positive charge of the metal ions affects negatively charged bacteria, especially *E. coli* . Accordingly, this interference leads to the inactivation of cellular enzymes and then the permeability of the membrane [125, 130, 131].

Table 3-7 The antibacterial activity of SiO₂@Cu(II) and SiO₂@Cu(0) against *E. coli* and *S. aureus* .

Copper-silica nanoparticles	Con. mg/mL	Inhibition zone(mm) of <i>E. coli</i> by SiO ₂ @Cu(II)	Inhibition zone(mm) of <i>E. coli</i> by SiO ₂ @Cu(0)
	100	24 ±3.38	30±2.13
	80	19 ±1.34	24± 1.704
	60	16.6± 1.17	21.5± 0.887
	40	12±0.852	15.5± 1.101
	20	6±0.845	7.5± 0.532
	Inhibition average	15.52± 1.517	19.7± 1.271
	L.S.D at 0.05	1.92	0.983
	DMSO	nill	nill
	Control positive (Ciprofloxacin) mm in diameter Antibiotic 5mg/disc	9	
Copper-silica nanoparticles	Con. mg/mL	Inhibition zone(mm) of <i>S. aureus</i> by SiO ₂ @Cu(II)	Inhibition zone(mm) of <i>S. aureus</i> by SiO ₂ @Cu(0)
	100	23± 1.67	28± 2.04
	80	18± 1.31	22± 1.61
	60	14± 1.02	18± 1.31
	40	10± 0.73	13± 0.95
	20	4± 0.292	5.5± 0.402
	Inhibition average	13.8± 1.014	17.5± 1.27
	L.S.D at 0.05	1.149	5.68
	Control positive (Ciprofloxacin) mm in diameter Antibiotic 5mg/disc	6	

Table 3-8 Minimum inhibitory concentration (MIC) mg/mL for SiO₂@Cu(II) and SiO₂@Cu(0) against *E. coli* and *S. aureus*..

Minimum inhibitory concentration(MIC) mg/mL against <i>E.Coli</i>						
Copper-silica nanoparticles	Concentration (mg/mL)					
	50	25	12.5	6.25	3.125	1.5625
SiO ₂ @Cu(II)	-	-	-	-	+	+
SiO ₂ @Cu(0)	-	-	-	-	-	+
Minimum inhibitory concentration(MIC) mg/mL against <i>S. aureus</i>						
Copper-silica nanoparticles	Concentration (mg/mL)					
	50	25	12.5	6.25	3.125	1.5625
SiO ₂ @Cu(II)	-	-	-	-	-	+
SiO ₂ @Cu(0)	-	-	-	-	-	+

- no growth + growth

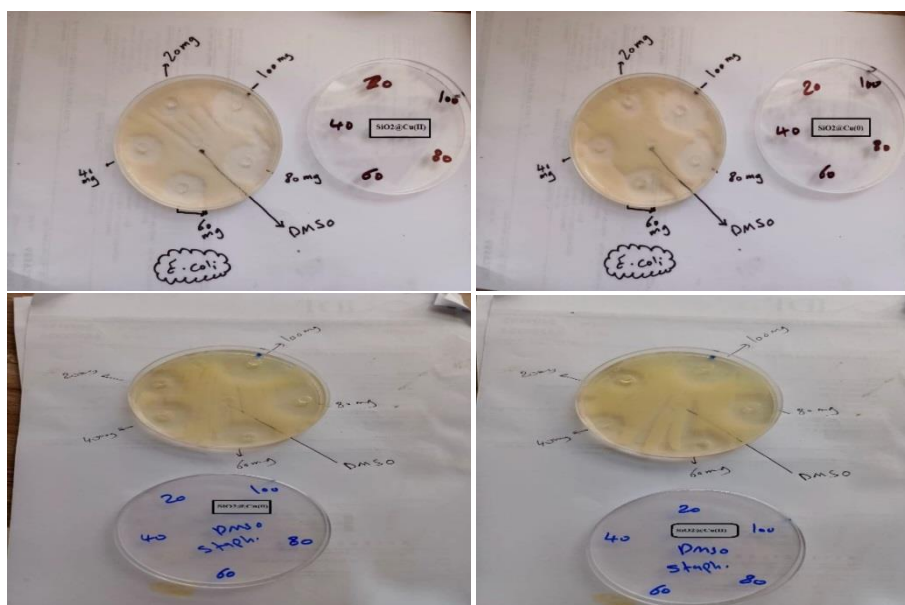


Figure.3.19 Antibacterial activity of nickel-silica nanoparticles SiO₂@Cu(II) and SiO₂@Cu(0) against *E.coli* and *S.aureus* in different concentrations 20, 40, 60, 80 and 100 mg/mL.

4 Conclusion

1. This study was based on the preparation of metals for nano composites that are used to inhibit types of bacteria *E.coli* and *S.aureus*.
2. The result showed that the prepared nickel and copper -silica nanoparticles are able to inhibit the growth of isolates of bacteria *E.coli* and *S.aureus*, isolated from infected individuals. This reveals the possibility of using these compound to treat these bacteria.
3. The nanocomposit $\text{SiO}_2\text{@Ni(II)}$ showed a high ability to inhibit bacteria *E.col* and *S.aureus*, through L.S.D value which reached 2.5 and 2.35 respectively. While the $\text{SiO}_2\text{@Ni(0)}$ composite showed its ability to inhibit bacteria *E.col* and *S.aureus* through L.S.D value of 2.19 and 2.04 resparadely.
4. The nano composite $\text{SiO}_2\text{@Cu(0)}$ showed a high ability to inhibit *S.aureus* bacteria through the L.S.D value which reached 5.68. Additionally, the nanocomposit $\text{SiO}_2\text{@Cu(II)}$ showed a high ability to inhibit *E.coli* bacteria through L.S.D value which reached 1.92.
5. The present study showed that nickel silica nanoparticles and copper silica nanoparticles $\text{SiO}_2\text{@Ni(II)}$, $\text{SiO}_2\text{@Ni(0)}$, $\text{SiO}_2\text{@Cu(II)}$ and $\text{SiO}_2\text{@Cu(0)}$ gave high inhibition compared to the antibiotic ciprofloxacin.

5 Future Works.

1. Preparation, characterization and the study of new silica-metal nanoparticles and employing it in many application such as catalysts and antimicrobial agents.
2. Extracting silica from various sources such as Banana, Bamboo and barley.
3. Studying the ability of nano composites to form biofilms for the bacteria under study.
4. Studying the efficieney of these compound prepared from rice husks on other pathogenic bacteria.
5. The possibility of adopting nanocomposites prepared from rice husks as alternatives to treatment with chemicals of side effects after testing them on laboratory animals.

References

References

1. Hello, K.M., Mihsen, H.H., Mosa, M.J.: Modification of silica with 2, 4-dinitrophenylhydrazanomethylphenol for monosaccharide productions. (2014)
2. Mohammed, K., Hamied, H., Jaafar, M.: Journal of the Taiwan Institute of Chemical Engineers Hydrolysis of cellulose over silica-salicylaldehyde phenylhydrazone catalyst. *J. Taiwan Inst. Chem. Eng.* 46, 74–81 (2015). <https://doi.org/10.1016/j.jtice.2014.09.005>
3. Khan, Y., Sattar, A., Ullah, S.A., Rehman, W., Khan, S., Hussain, R., Aslam, S., Rehman, Z.U., Nawaz, M., Gulshan, U.: Rice Husk Based Bio-composites. In: *Rice Husk Biomass: Processing, Properties and Applications*. pp. 235–270. Springer (2025)
4. Zhang, S., Gao, H., Li, J., Huang, Y., Alsaedi, A., Hayat, T., Xu, X., Wang, X.: Rice husks as a sustainable silica source for hierarchical flower-like metal silicate architectures assembled into ultrathin nanosheets for adsorption and catalysis. *J. Hazard. Mater.* 321, 92–102 (2017). <https://doi.org/10.1016/j.jhazmat.2016.09.004>
5. Mihsen, H.H., Al-Hasani, T.J., Hello, K.M.: Preparation of nanoporous material containing sulfide-carboxyl group derived from rice plant. In: *AIP Conference Proceedings* (2020)
6. Mihsen, H.H., Rfaish, S.Y., Abass, S.K., Sobh, H.S.: Synthesis and characterization of silica-thioamide hybrid compounds derived from rice husk ash with expected biological and catalytic activity. *J. Glob. Pharma Technol.* 10, 590–598 (2018)
7. Hoshida, H., Tanaka, Y., Hibino, T., Hayashi, Y., Tanaka, A., Takabe, T., Takabe, T.: Enhanced tolerance to salt stress in transgenic rice that

- overexpresses chloroplast glutamine synthetase. *Plant Mol. Biol.* 43, 103–111 (2000). <https://doi.org/10.1023/A:1006408712416>
8. Jin, W., Xu, W., Liang, H., Li, Y., Liu, S., Li, B.: *Nanoemulsions for food: properties, production, characterization, and applications*. Elsevier Inc. (2016)
 9. Jal, P.K., Patel, S., Mishra, B.K.: Chemical modification of silica surface by immobilization of functional groups for extractive concentration of metal ions. *Talanta*. 62, 1005–1028 (2004). <https://doi.org/10.1016/j.talanta.2003.10.028>
 10. Bakar, R.A., Yahya, R., Gan, S.N.: Production of high purity amorphous silica from rice husk. *Procedia Chem.* 19, 189–195 (2016)
 11. Nur Kamilah, M., Khalik, W.M.A.W.M., Azmi, A.A.: Synthesis and characterization of silica-silver core-shell nanoparticles. *Malaysian J. Anal. Sci.* 23, 290–299 (2019). <https://doi.org/10.17576/mjas-2019-2302-13>
 12. Fernandes, I.J., Calheiro, D., Sánchez, F.A.L., Camacho, A.L.D., De Campos Rocha, T.L.A., Moraes, C.A.M., De Sousa, V.C.: Characterization of silica produced from rice husk ash: Comparison of purification and processing methods. *Mater. Res.* 20, 519–525 (2017). <https://doi.org/10.1590/1980-5373-mr-2016-1043>
 13. Mohamed, R.M., Mkhallid, I.A., Barakat, M.A.: Rice husk ash as a renewable source for the production of zeolite NaY and its characterization. *Arab. J. Chem.* 8, 48–53 (2015). <https://doi.org/10.1016/j.arabjc.2012.12.013>
 14. Zopener_8a4800Ea0a3F43F4Bafd7706C1a4E7Ee
 15. Chik, N.S.I., Shaari, N.Z.K., Ramlee, N.A., Manaf, M.R.A.: Extraction of

- silica from rice husk ash and its effect on the properties of the integral membrane. *ASM Sci. J.* 17, 1–13 (2022)
16. Prawingwong, P., Chaiya, C., Reubroycharoen, P., Samart, C.: Utilization of rice husk ash silica in controlled releasing application. *J. Met. Mater. Miner.* 19, 61–65 (2009)
 17. Zarei, V., Mirzaasadi, M., Davarpanah, A., Nasiri, A., Valizadeh, M., Hosseini, M.J.S.: Environmental method for synthesizing amorphous silica oxide nanoparticles from a natural material. *Processes.* 9, 334 (2021)
 18. Şimşek, Y.E.: Preparation and characterization of high purity silica obtained from rice husks. *Acta Phys. Pol. A.* 132, 1002–1005 (2017).
<https://doi.org/10.12693/APhysPolA.132.1002>
 19. Sobh, H.S., Mihsen, H.H.: Synthesis of Functionalized Silica from Rice Husks Containing C-I End Group. *Baghdad Sci. J.* 16, 0886 (2019).
<https://doi.org/10.21123/bsj.2019.16.4.0886>
 20. Alguns, R.D.E., Soluções, Í.D.E.: SYNTHESIS OF NEW ADSORBENTS VIA FUNCTIONALIZED MCM-41 FOR THE. 21, 42–60 (2024).
<https://doi.org/10.52571/PTQ.v21.n47.2024>
 21. Gupta, R.P.: Electronic structure of crystalline and amorphous silicon dioxide. *Phys. Rev. B.* 32, 8278–8292 (1985).
<https://doi.org/10.1103/PhysRevB.32.8278>
 22. Fernández, L.D., Lara, E., Mitchell, E.A.D.: Checklist, diversity and distribution of testate amoebae in Chile. *Eur. J. Protistol.* 51, 409–424 (2015). <https://doi.org/10.1016/j.ejop.2015.07.001>
 23. Li, Y.P., Ching, W.Y.: Band structures of all polycrystalline forms of silicon dioxide. *Phys. Rev. B.* 31, 2172–2179 (1985).

<https://doi.org/10.1103/PhysRevB.31.2172>

24. Nazopatul, P.H., Irmansyah, Irzaman: Extraction and characterization of silicon dioxide from rice straw. In: IOP Conference Series: Earth and Environmental Science. p. 12013. IOP Publishing (2018)
25. Castellari, M., Versari, A., Fabiani, A., Parpinello, G.P., Galassi, S.: Removal of ochratoxin A in red wines by means of adsorption treatments with commercial fining agents. *J. Agric. Food Chem.* 49, 3917–3921 (2001)
26. Shafiey Dehaj, M., Zamani Mohiabadi, M.: Experimental study of water-based CuO nanofluid flow in heat pipe solar collector. *J. Therm. Anal. Calorim.* 137, 2061–2072 (2019). <https://doi.org/10.1007/s10973-019-08046-6>
27. Singh, L.P., Agarwal, S.K., Bhattacharyya, S.K., Sharma, U., Ahalawat, S.: Preparation of silica nanoparticles and its beneficial role in cementitious materials. *Nanomater. Nanotechnol.* 1, 9 (2011)
28. Oh, K., Paek, U.-C.: *Silica optical fiber technology for devices and components: design, fabrication, and international standards.* John Wiley & Sons (2012)
29. Liou, T.H., Yang, C.C.: Synthesis and surface characteristics of nanosilica produced from alkali-extracted rice husk ash. *Mater. Sci. Eng. B.* 176, 521–529 (2011). <https://doi.org/10.1016/j.mseb.2011.01.007>
30. Gun, M., Arslan, H., Saleh, M., Yalvac, M., Dizge, N.: Optimization of silica extraction from rice husk using response surface methodology and adsorption of safranin dye. *Int. J. Environ. Res.* 16, 20 (2022)
31. Nath, N., Chakroborty, S., Panda, P., Pal, K.: High yield silica-based emerging nanoparticles activities for hybrid catalyst applications. *Top.*

- Catal. 65, 1706–1718 (2022)
32. Mohsin, A.D., Mihsen, H.H.: Uptake of Metal Ions (Co(II) and Ni(II)) by Silica-Salicylaldehyde Derived from Rice Husks. *J. Inorg. Organomet. Polym. Mater.* 30, 2172–2181 (2020). <https://doi.org/10.1007/s10904-019-01379-7>
 33. Haider, J. Bin, Haque, M.I., Hoque, M., Hossen, M.M., Mottakin, M., Khaleque, M.A., Johir, M.A.H., Zhou, J.L., Ahmed, M.B., Zargar, M.: Efficient extraction of silica from openly burned rice husk ash as adsorbent for dye removal. *J. Clean. Prod.* 380, 135121 (2022)
 34. Hoffmann, F., Cornelius, M., Morell, J., Fröba, M.: Silica-based mesoporous organic-inorganic hybrid materials. *Angew. Chemie - Int. Ed.* 45, 3216–3251 (2006). <https://doi.org/10.1002/anie.200503075>
 35. Tariq, A., Mihsen, H.H., Saeed, S.I., Eesa, M.T.: Synthesis of Organic–Inorganic Hybrid Magnetic Material for Removal of Co(II), Ni(II) and Cu(II) Ions from its Aqueous Solutions. *J. Inorg. Organomet. Polym. Mater.* (2024). <https://doi.org/10.1007/s10904-024-03247-5>
 36. Mohsin, A.D., Mihsen, H.H.: Uptake of metal ions (Co (II) and Ni (II)) by silica-salicylaldehyde derived from rice husks. *J. Inorg. Organomet. Polym. Mater.* 30, 2172–2181 (2020)
 37. Dhahir, A., Hayder, M., Mihsen, H.: Uptake of Metal Ions (Co (II) and Ni (II)) by Silica - Salicylaldehyde Derived from Rice Husks. *J. Inorg. Organomet. Polym. Mater.* (2019). <https://doi.org/10.1007/s10904-019-01379-7>
 38. Abbas, S.K., Hassan, Z.M., Mihsen, H.H., Eesa, M.T., Attol, D.H.: Uptake of Nickel(II) Ion by Silica-o-Phenylenediamine Derived from Rice Husk Ash. *Silicon.* 12, 1103–1110 (2020). <https://doi.org/10.1007/s12633-019->

39. Sereda, L., Visconte, L.L.Y., Nunes, R.C.R., Furtado, C.R.G., Riande, E.: Effect of silica and rice husk ash fillers on the modulus of polysiloxane networks. *J. Appl. Polym. Sci.* 90, 421–429 (2003)
40. Li, Z., Chen, Z., Liu, J., Fu, Y., Liu, C., Wang, P., Jiang, M., Lao, C.: Additive manufacturing of lightweight and high-strength polymer-derived SiOC ceramics. *Virtual Phys. Prototyp.* 15, 1–15 (2020).
<https://doi.org/10.1080/17452759.2019.1710919>
41. Ni'mah, Y.L., Muhaiminah, Z.H., Suprpto, S.: Synthesis of silica nanoparticles from sugarcane bagasse by sol-gel method. In: *AIP Conference Proceedings*. AIP Publishing (2023)
42. Liou, T.-H.: Preparation and characterization of nano-structured silica from rice husk. *Mater. Sci. Eng. A.* 364, 313–323 (2004)
43. Nayak, J.P., Bera, J.: Preparation of silica aerogel by ambient pressure drying process using rice husk ash as raw material. *Trans. Indian Ceram. Soc.* 68, 91–94 (2009)
44. Chatterjee, M., Naskar, M.K.: Sol–gel synthesis of lithium aluminum silicate powders: the effect of silica source. *Ceram. Int.* 32, 623–632 (2006)
45. Sembiring, S., Simanjuntak, W., Manurung, P., Asmi, D., Low, I.M.: Synthesis and characterisation of gel-derived mullite precursors from rice husk silica. *Ceram. Int.* 40, 7067–7072 (2014)
46. Zuwana, I., Riza, M., Aprilia, S.: The impact of solvent concentration on the characteristic of silica from rice husk ash using sol gel method. In: *IOP Conference Series: Materials Science and Engineering*. p. 12060. IOP Publishing (2021)

47. Pandiangan, K.D., Simanjuntak, W., Pratiwi, E., Rilyanti, M.: Characteristics and catalytic activity of zeolite-a synthesized from rice husk silica and aluminium metal by sol-gel method. In: *Journal of Physics: Conference Series*. p. 12015. IOP Publishing (2019)
48. Durães, L., Ochoa, M., Rocha, N., Patrício, R., Duarte, N., Redondo, V., Portugal, A.: Effect of the drying conditions on the microstructure of silica based xerogels and aerogels. *J. Nanosci. Nanotechnol.* 12, 6828–6834 (2012). <https://doi.org/10.1166/jnn.2012.4560>
49. Simanjuntak, W., Sembiring, S., Pandiangan, K.D., Syani, F., Situmeang, R.: The use of liquid smoke as a substitute for nitric acid for extraction of amorphous silica from rice husk through sol-gel r. *Orient. J. Chem.* 32, 2079–2085 (2016)
50. Alhadhrami, A., Mohamed, G.G., Sadek, A.H., Ismail, S.H., Ebnalwaled, A.A., Almalki, A.S.A.: Behavior of silica nanoparticles synthesized from rice husk ash by the sol–gel method as a photocatalytic and antibacterial agent. *Materials (Basel)*. 15, 8211 (2022)
51. Zulkifli, N.S.C., Ab Rahman, I., Mohamad, D., Husein, A.: A green sol–gel route for the synthesis of structurally controlled silica particles from rice husk for dental composite filler. *Ceram. Int.* 39, 4559–4567 (2013)
52. Rahman, I.A., Padavettan, V.: Synthesis of Silica nanoparticles by Sol-Gel: Size-dependent properties, surface modification, and applications in silica-polymer nanocompositesa review, (2012)
53. Hassan, A.F., Abdelghny, A.M., Elhadidy, H., Youssef, A.M.: Synthesis and characterization of high surface area nanosilica from rice husk ash by surfactant-free sol–gel method. *J. sol-gel Sci. Technol.* 69, 465–472 (2014)
54. Le, V.H., Thuc, C.N.H., Thuc, H.H.: Synthesis of silica nanoparticles from

- Vietnamese rice husk by sol–gel method. *Nanoscale Res. Lett.* 8, 1–10 (2013)
55. Ali, H.H., Mihsen, H.H., Hussain, K.A.: Synthesis, Characterization and Antimicrobial Studies of Modified Silica Materials Derived from Rice Husks. *Bionanoscience*. 13, 1163–1176 (2023)
56. Setyawan, N., Yuliani, S.: Synthesis of silica from rice husk by sol-gel method. In: *IOP Conference Series: Earth and Environmental Science*. p. 12149. IOP Publishing (2021)
57. Ahangaran, F., Navarchian, A.H.: Recent advances in chemical surface modification of metal oxide nanoparticles with silane coupling agents: A review. *Adv. Colloid Interface Sci.* 286, 102298 (2020).
<https://doi.org/10.1016/j.cis.2020.102298>
58. Ellateif, A., Mohammad, T., Maitra, S.: Modification of Silica surface by Titanium sol synthesis and characterization. *Int. J. Nano Dimens.* 8, 187–196 (2017)
59. Sharma, R.K., Mittal, S., Azami, S., Adholeya, A.: Surface modified silica gel for extraction of metal ions: An environment friendly method for waste treatment. *Surf. Eng.* 21, 232–237 (2005).
<https://doi.org/10.1179/174329405X50082>
60. Yildirim, A., Demirel, G.B., Erdem, R., Senturk, B., Tekinay, T., Bayindir, M.: Pluronic polymer capped biocompatible mesoporous silica nanocarriers. *Chem. Commun.* 49, 9782–9784 (2013).
<https://doi.org/10.1039/c3cc45967e>
61. Fechete, I., Wang, Y., Védrine, J.C.: The past, present and future of heterogeneous catalysis. *Catal. Today*. 189, 2–27 (2012)

62. Peled, A., Pevzner, A., Peretz Soroka, H., Patolsky, F.: Morphological and chemical stability of silicon nanostructures and their molecular overlayers under physiological conditions: towards long-term implantable nanoelectronic biosensors. *J. Nanobiotechnology*. 12, 1–11 (2014)
63. Salama, T.M., Ali, I.O., Gumaa, H.A., Lateef, M.A., Bakr, M.F.: Novel synthesis of nay zeolite from rice husk silica: modification with ZnO and ZnS for antibacterial application. *Chem Sci J*. 7, 1–9 (2016)
64. Jasni, N., Iqbal, A., Bakar, N.H.H.A., Yanto, D.H.Y., Yi, H.J., Kaus, N.H.M., Ahmad, M.N., Mulijani, S.: Highly porous Bi (III) modified rice husk silica photocatalyst for the photocatalytic removal of cationic methylene blue. *Iran. J. Catal.* 13, (2023)
65. Li, Y., Zhao, M., Yan, H., Chen, Y., Liu, Y., Jiang, H., Chen, L., Hou, S., Chi, N., Jia, S.: Highly porous Bi (III) modified rice husk silica photocatalyst for the photocatalytic removal of cationic methylene blue. *J. Water Process Eng.* 60, 105218 (2024)
66. Malafatti, J.O.D., Tavares, F.A., Neves, T.R., Mascarenhas, B.C., Quaranta, S., Paris, E.C.: Modified Silica Nanoparticles from Rice Husk Supported on Polylactic Acid as Adsorptive Membranes for Dye Removal. *Materials (Basel)*. 16, 2429 (2023)
67. Hassan, S.A., Al-Sabagh, A.M., Shalaby, N.H., Hanafi, S.A., Hassan, H.A.: Various characteristics of multi-modified rice husk silica-anchored Ni or Pt nanoparticles as swift catalytic systems in some petrochemical processes. *J. Taiwan Inst. Chem. Eng.* 59, 484–495 (2016)
68. Cong, X., Tang, Z., Lu, S., Tan, Y., Wang, C., Yang, L., Shi, X.: Effect of rice husk ash surface modification by silane coupling agents on damping capacity of cement-based pastes. *Constr. Build. Mater.* 296, 123730 (2021)

69. Ayswarya, E.P., Nair, A.B., Thachil, E.T.: A comparative study of mechanical, dynamic mechanical and thermal properties of rice husk ash, modified rice husk ash and nano silica filled epoxy composites. *Mater. Today Proc.* 47, 5351–5357 (2021)
70. Adam, F., Fook, C.L.: Chromium modified silica from rice husk as an oxidative catalyst. *J. Porous Mater.* 16, 291–298 (2009)
71. Sadon, F.N., Ibrahim, A.S., Ismail, K.N.: An overview of rice husk applications and modification techniques in wastewater treatment. *J Purity Util. React. Env.* 1, 308–334 (2012)
72. Nuryono, N., Rosiati, N.M., Rusdiarso, B., Sakti, S.C.W., Tanaka, S.: Coating of magnetite with mercapto modified rice hull ash silica in a one-pot process. *Springerplus.* 3, 1–12 (2014)
73. Chandrasekhar, S., Satyanarayana, K.G., Pramada, P.N., Raghavan, P., Gupta, T.N.: Review processing, properties and applications of reactive silica from rice husk—an overview. *J. Mater. Sci.* 38, 3159–3168 (2003)
74. Chang, F.-W., Hsiao, T.-J., Shih, J.-D.: Hydrogenation of CO₂ over a rice husk ash supported nickel catalyst prepared by deposition–precipitation. *Ind. Eng. Chem. Res.* 37, 3838–3845 (1998)
75. Chang, F.-W., Hsiao, T.-J., Chung, S.-W., Lo, J.-J.: Nickel supported on rice husk ash—activity and selectivity in CO₂ methanation. *Appl. Catal. A Gen.* 164, 225–236 (1997)
76. Harasim, P., Filipek, T.: Nickel in the environment. *J. Elem.* 20, (2015)
77. Liu, X., Liu, Y., Shi, X., Yu, Z., Feng, L.: Synthesis and catalytic performance of SiO₂@Ni and hollow Ni microspher. *Appl. Phys. A Mater. Sci. Process.* 122, (2016). <https://doi.org/10.1007/s00339-016-0526-5>

78. Liu, R., Bray, P., Pollard, A.M., Hommel, P.: Chemical analysis of ancient Chinese copper-based objects: Past, present and future. *Archaeol. Res. Asia.* 3, 1–8 (2015)
79. Shimada, I., Merkel, J.F.: Copper-alloy metallurgy in ancient Peru. *Sci. Am.* 265, 80–87 (1991)
80. Craddock, P.T.: The composition of the copper alloys used by the Greek, Etruscan and Roman civilisations: 2. the Archaic, Classical and Hellenistic Greeks. *J. Archaeol. Sci.* 4, 103–123 (1977)
81. MIYAKE, Y.: A brief history of the copper metallurgy in ancient Western Asia. *J. MMIJ.* 124, 554–561 (2008)
82. Devan, R.S., Kolekar, Y.D., Chougule, B.K.: Effect of cobalt substitution on the properties of nickel–copper ferrite. *J. Phys. Condens. Matter.* 18, 9809 (2006)
83. Jarjoura, G., Muinonen, M., Kipouros, G.J.: Physicochemical properties of nickel copper sulfate solutions. *Can. Metall. Q.* 42, 281–288 (2003)
84. Khoshmaram, L., Saadati, M., Karimi, A.: A simple and rapid technique for the determination of copper based on air-assisted liquid–liquid microextraction and image colorimetric analysis. *Anal. Methods.* 12, 3490–3498 (2020)
85. Sánchez-López, E., Gomes, D., Esteruelas, G., Bonilla, L., Lopez-Machado, A.L., Galindo, R., Cano, A., Espina, M., Ettcheto, M., Camins, A.: Metal-based nanoparticles as antimicrobial agents: an overview. *Nanomaterials.* 10, 292 (2020)
86. Chatterjee, A.K., Chakraborty, R., Basu, T.: Mechanism of antibacterial activity of copper nanoparticles. *Nanotechnology.* 25, 135101 (2014)

87. Din, M.I., Khalid, R., Arshad, F., Hussain, Z., Batool, M.: Synthesis, Characterization and Antimicrobial Studies of Modified Silica Materials Derived from Rice Husks. *Inorg. Nano-Metal Chem.* 1–18 (2024)
88. Chirra, S., Siliveri, S., Gangalla, R., Goskula, S., Gujjula, S.R., Adepu, A.K., Anumula, R., Sivasoorian, S.S., Wang, L.F., Narayanan, V.: Synthesis of new multivalent metal ion functionalized mesoporous silica and studies of their enhanced antimicrobial and cytotoxicity activities. *J. Mater. Chem. B.* 7, 7235–7245 (2019). <https://doi.org/10.1039/c9tb01736d>
89. Wu, Y., Kong, L.: Advance on toxicity of metal nickel nanoparticles. *Environ. Geochem. Health.* 42, 2277–2286 (2020)
90. Gomez, G.E., Hamer, M., Regiart, M.D., Tortella, G.R., Seabra, A.B., Soler Illia, G.J.A.A., Fernández-Baldo, M.A.: Advances in Nanomaterials and Composites Based on Mesoporous Materials as Antimicrobial Agents: Relevant Applications in Human Health. *Antibiotics.* 13, 173 (2024)
91. Tay, C.Y., Setyawati, M.I., Xie, J., Parak, W.J., Leong, D.T.: Back to basics: Exploiting the innate physico-chemical characteristics of nanomaterials for biomedical applications. *Adv. Funct. Mater.* 24, 5936–5955 (2014). <https://doi.org/10.1002/adfm.201401664>
92. Argueta-Figueroa, L., Morales-Luckie, R.A., Scougall-Vilchis, R.J., Olea-Mejía, O.F.: Synthesis, characterization and antibacterial activity of copper, nickel and bimetallic Cu–Ni nanoparticles for potential use in dental materials. *Prog. Nat. Sci. Mater. Int.* 24, 321–328 (2014)
93. Chaudhary, J., Tailor, G., Yadav, B.L., Michael, O.: Synthesis and biological function of Nickel and Copper nanoparticles. *Heliyon.* 5, (2019)
94. Mamonova, I.A., Babushkina, I. V, Norkin, I.A., Gladkova, E. V, Matasov, M.D., Puchin'yan, D.M.: Biological activity of metal nanoparticles and

- their oxides and their effect on bacterial cells. *Nanotechnologies Russ.* 10, 128–134 (2015)
95. Jaji, N.-D., Lee, H.L., Hussin, M.H., Akil, H.M., Zakaria, M.R., Othman, M.B.H.: Advanced nickel nanoparticles technology: From synthesis to applications. *Nanotechnol. Rev.* 9, 1456–1480 (2020)
96. Kumar, H., Rani, R., Salar, R.: Reverse micellar synthesis, characterization & antibacterial study of nickel nanoparticles. *Adv. Control. Chem. Eng. Civ. Eng. Mech. Eng.* 88–94 (2010)
97. Sagadevan, S., Fatimah, I., Anita Lett, J., Rahman, M.Z., Leonard, E., Oh, W.-C.: Eco-friendly green approach of nickel oxide nanoparticles for biomedical applications. *Open Chem.* 21, 20230141 (2023)
98. Ali, H.H., Hussein, K.A., Mihsen, H.H.: Antimicrobial applications of nanosilica derived from rice grain husks. *Silicon.* 15, 5735–5745 (2023)
99. Ali, I., Said, M., AlWazn, W.: Preparation, Characterization, and Study of Complexes Containing Beta-lactam Group with Some Transitional Elements and their Biological Activity. *Egypt. J. Chem.* 64, 0–0 (2021).
<https://doi.org/10.21608/ejchem.2021.72890.3614>
100. Kavaz, D., Vaseashta, A.: Synthesizing nano silica nanoparticles from barley grain waste: effect of temperature on mechanical properties. *Polish J. Environ. Stud.* 28, (2019).
<https://doi.org/https://doi.org/10.15244/pjoes/91078>
101. Attol, D.H., Mihsen, H.H., Jaber, S.A., Alwazni, W.S., Eesa, M.T.: Synthesis of Organic Functionalized Silica from Rice Husk as an Antibacterial Agents. *Silicon.* 15, 2349–2357 (2023).
<https://doi.org/10.1007/s12633-022-02194-5>

102. Hatem, R.S., Hussain, A.F., Mihsen, H.H.: Green synthesis, characterization, and adsorption of Co(II) and Cu(II) ions from aqueous solution by mesoporous silica MCM-41. *Chem. Pap.* (2024). <https://doi.org/10.1007/s11696-024-03538-8>
103. Ghorbani-Choghamarani, A., Tahmasbi, B., Arghand, F., Faryadi, S.: Nickel Schiff-base complexes immobilized on boehmite nanoparticles and their application in the oxidation of sulfides and oxidative coupling of thiols as novel and reusable nano organometal catalysts. *RSC Adv.* 5, 92174–92183 (2015). <https://doi.org/10.1039/C5RA14974F>
104. Akhayere, E., Kavaz, D.: Nano-silica and nano-zeolite synthesized from barley grass straw for effective removal of gasoline from aqueous solution: a comparative study. *Chem. Eng. Commun.* 208, 1419–1435 (2021). <https://doi.org/10.1080/00986445.2020.1786373>
105. Hassan, S.A., Al-Sabagh, A.M., Shalaby, N.H., Hanafi, S.A., Hassan, H.A.: Catalytic performance of organically templated nano nickel incorporated-rice husk silica in hydroconversion of cyclohexene and dehydrogenation of ethanol. *Egypt. J. Pet.* 22, 179–188 (2013). <https://doi.org/10.1016/j.ejpe.2012.09.009>
106. Mihsen, H.H., Abass, S.K., Abed Alhasan, M.T., Hassan, Z.M., Abass, A.K.: Synthesis, Characterization and Antimicrobial Activities of Mixed Ligand Complexes of Fe (II), Co(II), Ni(II) and Cu (II) Ions Derived from Imine of Benzidine and o-phenylenediammine. *Iraqi J. Sci.* 61, 2762–2775 (2020). <https://doi.org/10.24996/ijs.2020.61.11.2>
107. AbuKhadra, M.R., Mohamed, A.S., El-Sherbeeney, A.M., Elmeligy, M.A.: Enhanced photocatalytic degradation of acephate pesticide over MCM-41/Co₃O₄ nanocomposite synthesized from rice husk silica gel and Peach

- leaves. *J. Hazard. Mater.* 389, 122129 (2020).
<https://doi.org/10.1016/j.jhazmat.2020.122129>
108. Gobara, H.M., Hassan, S.A.: A Comparative Study of Surface Characteristics of Nickel Supported on Silica Gel, γ -Alumina, Aluminosilicate. *Pet. Sci. Technol.* 27, 1555–1571 (2009).
<https://doi.org/10.1080/10916460802608677>
109. Li, Y., Lan, J.Y., Liu, J., Yu, J., Luo, Z., Wang, W., Sun, L.: Synthesis of gold nanoparticles on rice husk silica for catalysis applications. *Ind. Eng. Chem. Res.* 54, 5656–5663 (2015). <https://doi.org/10.1021/acs.iecr.5b00216>
110. Vargas, H., Morales, J.C., Bokhimi, X., Klimova, T.E.: Effect of the preparation method on the hydrogenation activity of Ni/SBA-15 catalysts: Comparison of EDTA complexation and DPU. *Catal. Today.* 305, 133–142 (2018). <https://doi.org/10.1016/j.cattod.2017.08.043>
111. Pimprom, S., Sriboonkham, K., Dittanet, P., Föttinger, K., Rupprechter, G., Kongkachuichay, P.: Synthesis of copper-nickel/SBA-15 from rice husk ash catalyst for dimethyl carbonate production from methanol and carbon dioxide. *J. Ind. Eng. Chem.* 31, 156–166 (2015).
<https://doi.org/10.1016/j.jiec.2015.06.019>
112. Alshook, N.A., Mihsen, H.H., Hanoon, H.D.: Synthesis and characterization of solid Brønsted acid derived from rice husks as an efficient catalyst for the preparation of some 2,4,5-trisubstituted imidazole derivatives. *Res. Chem. Intermed.* 50, 2581–2601 (2024).
<https://doi.org/10.1007/s11164-024-05281-x>
113. Adam, F., Hello, K.M., Chai, S.J.: The heterogenization of l-phenylalanine-Ru(III) complex and its application as catalyst in esterification of ethyl alcohol with acetic acid. *Chem. Eng. Res. Des.* 90, 633–642 (2012).

<https://doi.org/10.1016/j.cherd.2011.09.009>

114. Ariga, K., Vinu, A., Yamauchi, Y., Ji, Q., Hill, J.P.: Nanoarchitectonics for Mesoporous Materials. *Bull. Chem. Soc. Jpn.* 85, 1–32 (2012).
<https://doi.org/10.1246/bcsj.20110162>
115. Carraro, P.M., García Blanco, A.A., Chanquía, C., Sapag, K., Oliva, M.I., Eimer, G.A.: Hydrogen adsorption of nickel-silica materials: Role of the SBA-15 porosity. *Microporous Mesoporous Mater.* 248, 62–71 (2017).
<https://doi.org/10.1016/j.micromeso.2017.03.057>
116. Umegaki, T., Takei, C., Watanuki, Y., Xu, Q., Kojima, Y.: Fabrication of hollow nickel-silica composite spheres using l(+)-arginine and their catalytic performance for hydrolytic dehydrogenation of ammonia borane, (2013)
117. Sankarasubramanian, K., Soundarrajan, P., Logu, T., Sethuraman, K., Ramamurthi, K.: Enhancing resistive-type hydrogen gas sensing properties of cadmium oxide thin films by copper doping. *New J. Chem.* 42, 1457–1466 (2018). <https://doi.org/10.1039/c7nj03095a>
118. Biju, V.: Ni 2p X-ray photoelectron spectroscopy study of nanostructured nickel oxide. *Mater. Res. Bull.* 42, 791–796 (2007).
<https://doi.org/10.1016/j.materresbull.2006.10.009>
119. Wang, J., Gili, A., Grünbacher, M., Praetz, S., Epping, J.D., Görke, O., Schuck, G., Penner, S., Schlesiger, C., Schomäcker, R., Gurlo, A., Bekheet, M.F.: Silicon oxycarbonitride ceramic containing nickel nanoparticles: From design to catalytic application. *Mater. Adv.* 2, 1715–1730 (2021).
<https://doi.org/10.1039/d0ma00917b>
120. Yadav, H.M., Otari, S. V, Koli, V.B., Mali, S.S., Hong, C.K., Pawar, S.H., Delekar, S.D.: Preparation and characterization of copper-doped anatase

- TiO₂ nanoparticles with visible light photocatalytic antibacterial activity. *J. Photochem. Photobiol. A Chem.* 280, 32–38 (2014).
<https://doi.org/10.1016/j.jphotochem.2014.02.006>
121. Chen, J., Wei, Y., Yang, X., Ni, S., Hong, F., Ni, S.: Construction of selenium-embedded mesoporous silica with improved antibacterial activity. *Colloids Surfaces B Biointerfaces.* 190, 110910 (2020).
<https://doi.org/10.1016/j.colsurfb.2020.110910>
122. Tegegne, M., Abiyu, E., Libesu, S., Bedemo, B., Lewoyehu, M.: Phytochemical investigation, antioxidant and antibacterial activities of the fruit extracts of *Solanum anguivi*. *Biotechnol. Biotechnol. Equip.* 35, 1480–1491 (2021). <https://doi.org/10.1080/13102818.2021.1993087>
123. Zhang, F., You, X., Zhu, T., Gao, S., Wang, Y., Wang, R., Yu, H., Qian, B.: Silica nanoparticles enhance germ cell apoptosis by inducing reactive oxygen species (ROS) formation in *Caenorhabditis elegans*. *J. Toxicol. Sci.* 45, 117–129 (2020). <https://doi.org/10.2131/jts.45.117>
124. Selvarajan, V., Obuobi, S., Ee, P.L.R.: Silica Nanoparticles—A Versatile Tool for the Treatment of Bacterial Infections. *Front. Chem.* 8, 1–16 (2020).
<https://doi.org/10.3389/fchem.2020.00602>
125. Unglaube, F., Lammers, A., Kreyenschulte, C.R., Lalk, M., Mejía, E.: Preparation, Characterization and Antimicrobial Properties of Nanosized Silver-Containing Carbon/Silica Composites from Rice Husk Waste. *ChemistryOpen.* 10, 1244–1250 (2021)
126. Parida, K.M., Rath, D., Dash, S.S.: Synthesis, characterization and catalytic activity of copper incorporated and immobilized mesoporous MCM-41 in the single step amination of benzene. *J. Mol. Catal. A Chem.* 318, 85–93 (2010). <https://doi.org/10.1016/j.molcata.2009.11.011>

127. Zhang, G., Long, J., Wang, X., Zhang, Z., Dai, W., Liu, P., Li, Z., Wu, L., Fu, X.: Catalytic role of Cu sites of Cu/MCM-41 in phenol hydroxylation, (2010)
128. Shimokawabe, M., Takezawa, N., Kobayashi, H.: Characterization of copper-silica catalysts prepared by ion exchange. *Appl. Catal.* 2, 379–387 (1982)
129. Sondi, I., Salopek-Sondi, B.: Silver nanoparticles as antimicrobial agent: a case study on *E. coli* as a model for Gram-negative bacteria. *J. Colloid Interface Sci.* 275, 177–182 (2004)
130. Song, J., Kim, H., Jang, Y., Jang, J.: Enhanced antibacterial activity of silver/polyrhodanine-composite-decorated silica nanoparticles. *ACS Appl. Mater. Interfaces.* 5, 11563–11568 (2013)
131. Shanmugan, S., Ramalingam, R.J., Mutharasu, D.: Antibacterial activity and electrical properties of gold nanoparticle doped ceria-rice husk silica (Au/Ce-Silica) nanocomposites derived from biomass. *Synth. React. Inorganic, Met. Nano-Metal Chem.* 45, 304–308 (2015).
<https://doi.org/10.1080/15533174.2013.831897>

الخلاصة

تضمنت هذه الدراسة استخدام قشور الأرز لإنتاج أربعة مركبات نانوية من جسيمات السيليكا المعدنية ((SiO₂@Cu(0)، (SiO₂@Cu(II)، (SiO₂@Ni(0)، (SiO₂@Ni(II)) ذات قدرة عالية على تثبيط نوعين من البكتيريا الإشريكية القولونية (E.Coli) والمكورات العنقودية الذهبية (S.aureus) الضارة بصحة الإنسان.

في الخطوة الأولى تم تحضير محلول سيليكات الصوديوم من قشور ثم توظيف السيليكا بايونات النيكل والنحاس الثنائية من خلال اضافة سداسي هيدرات نترات النيكل لإنتاج SiO₂@Ni(II) وثلاثي هيدرات نترات النحاس لإنتاج SiO₂@Cu(II)- عبر طريقة السول-جل بعدها تم اختزال المركبات المحضرة بعامل مختزل هو بورهيدريد الصوديوم لتحضير الجسيمات النانوية SiO₂@Ni(0) و SiO₂@Cu(0) . شخضت المركبات المحضرة باستخدام عدة تقنيات (AFM، XPS، FESEM-EDX، XRD، FTIR) ، TEM، و(TGA/DTA). تم جمع عينات من البكتيريا المعزولة باستخدام الطرق التقليدية من مستشفى الحسيني التعليمي في كربلاء المقدسة وتم تشخيص هذه السلالات كيميائياً باستخدام نظام API staph المطبق وفقاً لتعليمات الشركة المصنعة. تم اختبار المركبات النانوية المحضرة من قشور الأرز RH-SiO₂@Ni(II)، SiO₂@Ni(0)، SiO₂@Cu(II) و SiO₂@Cu(0) ضد البكتيريا (E.Coli) و S.aureus بتركيزات مخففة (20، 40، 60، 80، 100) ملجم وبالمقارنة مع DMSO كعنصر تحكم سلبي. وقد تبين أن التأثير المثبط للمركبات المدروسة يزداد مع زيادة التركيز. كما تبين أن نمو بكتيريا يحدث عند تراكيز منخفضة من الجسيمات النانوية مقارنة بالمركبات المدروسة عند تراكيز عالية. من أقطار التثبيط، يبدو أن التثبيط بكتيريا S. aureus أعلى إلى حد ما من تثبيط بكتيريا E. coli.



جامعة كربلاء

كلية العلوم

قسم الكيمياء

تحضير و تشخيص مركبات السيليكا النانوية بواسطة طريقة السول-جل ودراسة فعاليتها البايولوجيه

رسالة

مقدمة لكلية العلوم / جامعة كربلاء وهي جزء من متطلبات نيل درجة الماجستير في علوم الكيمياء

كتب بواسطة

خضير رشيد كتاب

بكالوريوس. كيمياء (2007) / جامعة كربلاء

يشرف عليها

الأستاذ الدكتور. حيدر حميد محسن

1446 هجري

2025 ميلادي